

AD733490

HIGH PRESSURE SHOCK WAVE ATTENUATION

by
A. R. McMillan
W. M. Isbell
A. H. Jones

Materials and Structures Laboratory
Manufacturing Development, General Motors Corporation
General Motors Technical Center, Warren, Michigan 48090

D D C
RECEIVED
DEC 3 1971
RECEIVED
B

Reproduced by
**NATIONAL TECHNICAL
INFORMATION SERVICE**
Springfield, Va. 22151

DOCUMENT CONTROL DATA - R & D

(Security classification of title, body of abstract and indexing annotation must be entered when the overall report is classified)

1. ORIGINATING ACTIVITY (Corporate author)		2a. REPORT SECURITY CLASSIFICATION	
Manufacturing Development, General Motors Corporation, GM Technical Center, Warren, Michigan 48090		UNCLASSIFIED	
3. REPORT TITLE		2b. GROUP	
High Pressure Shock Wave Attenuation			
4. DESCRIPTIVE NOTES (Type of report and inclusive dates)			
Final Report			
5. AUTHOR(S) (First name, middle initial, last name)			
Allan R. McMillan, William M. Isbell, Arfon H. Jones			
6. REPORT DATE	7a. TOTAL NO. OF PAGES	7b. NO OF REFS	
1971, June	80	19	
8a. CONTRACT OR GRANT NO	9a. ORIGINATOR'S REPORT NUMBER(S)		
DA-49-146-XZ-322	Manufacturing Development		
b. PROJECT NO.	General Motors Corporation		
ARPA Order No. 560	MSL-70-01		
c.	9b. OTHER REPORT NO(S) (Any other numbers that may be assigned this report)		
Program Code 7E20	DASA 2425		
d.			
10. DISTRIBUTION STATEMENT			
Approved for Public Release; Distribution Unlimited			
11. SUPPLEMENTARY NOTES		12. SPONSORING MILITARY ACTIVITY	
		Advanced Research Projects Agency 1400 Wilson Blvd. Arlington, Virginia 22209	
13. ABSTRACT			
<p>The attenuation of high pressure shock waves has been investigated. High purity copper, 6061-T6 aluminum, 6Al-4V and α phase titanium, an uranium alloy and two alloys of beryllium were examined experimentally at pressures as high as 3 megabars. Low pressure experiments were instrumented with a velocity laser interferometer. Intermediate pressures (to several hundred kilobars) were instrumented with manganin wire piezoresistive gages and high pressure measurements were made through observation of free surface velocities.</p> <p>The results show that evidence of strength, as exhibited by elastic release wave behavior, persists to pressures of hundreds of kilobars and that the release wave structure is not elastic-perfectly plastic. For the materials examined the release wave structures can be described as exhibiting a Bauschinger effect. For megabar pressures (beyond melting behind the shock front) fluid behavior is indicated by the lack of an elastic release wave.</p>			

14. KEY WORDS	LINK A		LINK B		LINK C	
	ROLE	WT	ROLE	WT	ROLE	WT
Shock Wave Attenuation Material Strength Manganin Gages Elastic Release Wave Plastic Release Wave						

HIGH PRESSURE SHOCK WAVE ATTENUATION

"This work was supported by the Advanced Research Projects Agency
under ARPA Order No.560, Program Code 7E20"

by
A. R. McMillan
W. M. Isbell
A. H. Jones

Materials and Structures Laboratory
Manufacturing Development, General Motors Corporation
General Motors Technical Center, Warren, Michigan 48090

• PRESENTLY AT U.S. ARMY MATERIALS & MECHANICS RESEARCH CENTER WATERTOWN, MASSACHUSETTS 02172

prepared for
Advanced Research Projects Agency
1400 Wilson Blvd., Arlington, Virginia 22209

Under Contract No. DA-49-146-XZ-322

"Approved for public release; distribution unlimited"

BLANK PAGE

ABSTRACT

The attenuation of high pressure shock waves has been investigated. High purity copper, 6061-T6 aluminum, 6Al-4V and α phase titanium, an uranium alloy and two alloys of beryllium were examined experimentally at pressures as high as 3 megabars. Low pressure experiments were instrumented with a velocity laser interferometer. Intermediate pressures (to several hundred kilobars) were instrumented with manganin wire piezoresistive gages and high pressure measurements were made through observation of free surface velocities.

The results show that evidence of strength, as exhibited by elastic release wave behavior, persists to pressures of hundreds of kilobars and that the release wave structure is not elastic-perfectly plastic. For the materials examined the release wave structures can be described as exhibiting a Bauschinger effect. For megabar pressures (beyond melting behind the shock front) fluid behavior is indicated by the lack of an elastic release wave.

MSL-70-01

TABLE OF CONTENTS

	<u>Page</u>
LIST OF ILLUSTRATIONS	v
INTRODUCTION	1
SECTION I - EXPERIMENTAL TECHNIQUES	4
Launching Techniques	4
Instrumentation	8
SECTION II - DESCRIPTION OF IMPACT EXPERIMENTS	10
Design of Experiments	10
Laser Velocity Interferometer	11
Manganin Wire Gage	15
Stopped Targets	17
Wedge Targets	25
SECTION III - EXPERIMENTAL RESULTS	32
OFHC Copper	32
6061-T6 Aluminum	46
Titanium	56
Beryllium	62
Uranium Alloy	64
SECTION IV - CONCLUSIONS	66
REFERENCES	71
DISTRIBUTION LIST	73
DD FORM 1473 DOCUMENT CONTROL DATA R&D	79

LIST OF ILLUSTRATIONS

<u>Figure</u>		<u>Page</u>
1	Loading and Unloading for an Elastic-Perfectly Plastic Material	1
2	Layout of Light Gas Gun Range	5
3	Target Chamber	7
4	Top View of Target Chamber	7
5	X-Ray Shadowgraphs of Projectile Before Impact	9
6	Elastic Release Wave Velocity vs Shock Velocity for Several Materials	12
7	Manganin Wire Gage Construction	16
8	χ -t Diagram of Shock-Rarefaction System	19
9	Step Target Design	20
10	Step Target Technique	21
11	Free Surface Velocity vs Particle Velocity for Copper	23
12	Free Surface Velocity vs Particle Velocity for Aluminum	24
13	Wedge Target Design	26
14	Wedge Streak Camera Record for Copper-1.192 mm/ μ sec Impact Velocity, Pulse Length 0.20 μ sec	27
15	Distance-Time Record from Copper Wedge Record	29
16	Delta Time vs Distance from Copper Wedge Record	30
17	Velocity vs Distance from Copper Wedge Record	31
18	Copper Interferometer Records	34

MSL-70-01

LIST OF ILLUSTRATIONS (Continued)

<u>Figure</u>		<u>Page</u>
19	Copper Manganin Wire Record	36
20	Free Surface Velocity vs Distance for Copper from Manganin Wire Gage Record	38
21	Copper Stress-Strain Release Paths from Manganin Wire Gage Records	39
22	Free Surface Velocity vs Distance for Copper-2.5 mm/ μ sec Impact Velocity, Normalized to $U_{fs}=2.5$ mm/ μ sec at $X/X_0=2$, Pulse Length 0.17 μ sec	41
23	Free Surface Velocity vs Distance for Copper-7.3 mm/ μ sec Impact Velocity, Normalized to $U_{fs}=8.2$ mm/ μ sec at $X/X_0=2$, Pulse Length 0.16 μ sec	42
24	Normalized Attenuation for Copper	43
25	Release Wave Velocity vs Compression for Copper	45
26	Aluminum Manganin Wire Records	47
27	Free Surface Velocity vs Distance for Aluminum from Manganin Wire Gage Records	49
28	Aluminum Stress-Strain Release Paths from Manganin Wire Gage Records	50
29	Free Surface Velocity vs Distance Aluminum-2.5 mm/ μ sec Impact Velocity, Normalized to $U_{fs}=2.5$ at $X/X_0=2$, Pulse Length 0.14 μ sec	52
30	Normalized Attenuation for Aluminum	53
31	Release Wave Velocity vs Compression for Aluminum	55
32	α Titanium Manganin Wire Record	57

LIST OF ILLUSTRATIONS (Continued)

<u>Figure</u>		<u>Page</u>
33	α Titanium Stress-Strain Release Path from Manganin Wire Gage Record	58
34	Free Surface Velocity vs Distance for Titanium-2.6 mm/ μ sec Impact Velocity, Normalized to $U_{fs}=2.6$ at $X/X_0=2$, Pulse Length 0.17 μ sec	60
35	Release Wave Velocity vs Compression for Titanium	61
36	Free Surface Velocity vs Distance for Beryllium-2.5 mm/ sec Impact Velocity, Normalized to $U_{fs}=2.5$ at $X/X_0=1$, Pulse Length 0.11 μ sec	63
37	Free Surface Velocity vs Distance for Uranium Alloy-2.5 mm/ μ sec Impact Velocity, Normalized to $U_{fs}=2.5$ at $X/X_0=2$, Pulse Length 0.23 μ sec	65
38	Initial Release Wave Velocity vs Plastic Release Wave Velocity	67

INTRODUCTION

It is well known that most solids exhibit an elastic-plastic form of behavior when subjected to high speed loading by moderate strength shock waves, i.e. from the hugoniot elastic limit up to the order of 100 kilobars (1 kilobar = 10^9 dynes/cm²). At higher pressures the plastic wave velocity exceeds that of the elastic wave and only a plastic loading wave is observed. It is also expected that materials exhibiting elastic-plastic behavior on loading would show elastic-plastic behavior upon unloading. This is illustrated in Figure 1 which shows the stress-strain behavior for the theoretical model of an elastic-perfectly plastic material.

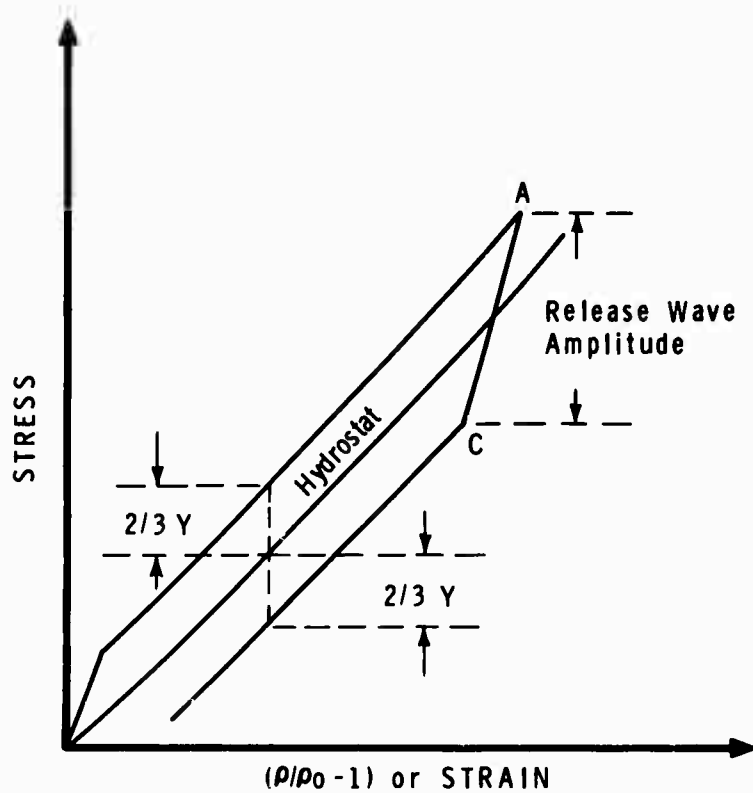


Figure 1 Loading and Unloading for an Elastic-Perfectly Plastic Material

MSL-70-01

For such a material the loading path lies $2/3 Y$ (Y is the yield strength) above the hydrostatic curve and is followed to the peak stress point, A. The initial release path is AC and an elastic wave of that amplitude is generated. The slope of AC is $(K + 4/3 G)$ where K is the bulk modulus and G is the shear modulus while the slope of the hydrostat is K . The release wave velocity is then

$$C = \sqrt{\frac{(K + 4/3 G)}{\rho}} \quad (1)$$

where ρ is the density of the material. The unloading from the point C is then plastic.

The question arises as to what degree this model matches experimental evidence. Several phenomena may be expected to modify this behavior. Many materials show strain rate sensitivity, i.e., increased resistance to deformation with increased rate of deformation. This could be exhibited by increased yield strength upon loading and release. The Bauschinger effect on release (an initially small yield strength followed by a rapid, then a slow increase) would be to spread the elastic rarefaction. If the pressure is great enough the material behind the shock front will be molten and no elastic rarefaction would be expected. Therefore, the purpose of this work has been to investigate the release wave behavior of several metals from high pressures in an effort to provide experimental information on the basic behavior of metals at high pressure.

Attenuation of high pressure shock waves has been studied previously by several investigators. Al'tshuler, et al.⁽¹⁾, measured elastic release wave velocities at low pressures and

pleastic release wave velocities at high pressures by various methods. Curran⁽²⁾ explained the results of his aluminum free surface velocity experiments in terms of an elastic release with the elastic yield increasing with pressure. Erkman and Christensen⁽³⁾ describe similar experiments with alloys of aluminum and concluded that the shear modulus may reach a maximum value at pressures between 100 and 340 kbars. Although mention is made, no conclusion is reached of the Bauschinger effect. Barker⁽⁴⁾ utilized the velocity interferometer to observe release waves in aluminum from pressures up to 90 kbars. He concluded the indistinct elastic-plastic structures of the observed release waves could be best described through the Bauschinger effect.

More recent observations have been made by Kusubov and VanThiel⁽⁵⁾ and Fuller and Price⁽⁶⁾ utilizing manganin wire gages. These gages are capable of recording pressure as a function of time at one location within the material being examined. From both these studies it can be concluded that elastic unloading occurs in alloys of aluminum and magnesium up to pressures of ~200 kbars. The magnitude of the elastic release wave indicates an increase of effective yield strength with pressure in this range.

With the exception of the work Al'tshuler, et al.⁽¹⁾, and Fuller and Price⁽⁶⁾ all work has been performed with alloys of aluminum. The work described herein details the investigation of shock wave attenuation of five metals and their alloys over a large range of pressures with the most accurate instrumentation techniques available. Thus an alloy of aluminum (6061-T6), pure copper, titanium (6Al-4V and pure in the α phase), two types of beryllium alloys (S-200 and a wrought alloy) and an uranium alloy were examined at pressures up to 3 Mbars.

MSL-70-01

SECTION I

EXPERIMENTAL TECHNIQUES

LAUNCHING TECHNIQUES

The technique used to launch flat impactor plates at prescribed velocities has been described previously in several reports. The essentials of these descriptions are repeated here for completeness.

The gun used to accelerate the impactor is an accelerated-reservoir light-gas gun with a launch tube bore diameter of either 29 mm or 69 mm. This type of gun maintains a reasonably constant pressure on the base of the projectile during the launch allowing the acceleration of a variety of unshocked impactor materials. Figure 2 shows the layout of the range.

The gun consists of the following major components.

1. Powder chamber.
2. Pump tube, 87 mm inside diameter by 12 m long.
3. Accelerated-reservoir high-pressure coupling.
4. Launch tube, either 29 mm inside diameter by 8 m long or 69 mm inside diameter and 8 m long.
5. Instrumented target chamber and flight range.

When the gun is loaded for firing, a weighted plastic-nosed piston is placed in the breech of the pump tube. Gun powder is then loaded in to the powder chamber behind the piston and

MSL-70-01

the pump tube is filled to the required pressure with hydrogen. After ignition of the gun powder, the hydrogen is compressed into the coupling by the accelerated piston. The saboted impactor is in turn accelerated by the release of the compressed hydrogen through a high pressure burst diaphragm.

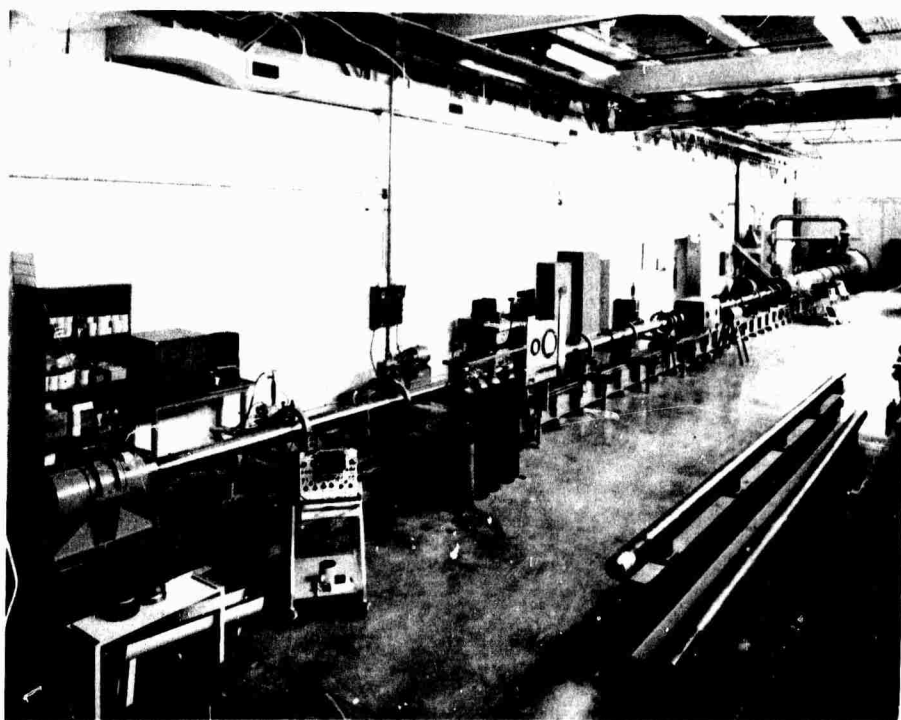


Figure 2 Layout of Light Gas Gun Range

MSL-70-01

Prior to firing, the flight range and instrument chamber are evacuated and then flushed with helium to approximately 10^{-2} torr to eliminate any spurious effects of gas build-up and ionization between projectile and target. Sealing lips on the rear of the plastic sabot are pressed tightly against the inside of the launch tube bore by an interference fit and the high pressure gas, effectively eliminating blow-by.

Careful attention to the condition of the launch tube is necessary for successful firing in the high velocity ranges. Bore linearity of better than 0.2 mm over the full 8 m length of the launch tube is maintained. The internal diameter is maintained to within 0.01 mm. Launch tubes are cleaned and honed after each firing and are removed every 15 to 20 firings for thorough reconditioning.

Figures 3 and 4 show the instrumentation chamber designed for the high pressure studies. The chamber is connected to the barrel of the gun only through an O-ring seal to allow free axial movement of the launch tube. The target chamber is shock-mounted to prevent target displacement before projectile impact. To facilitate this, several stages of mechanical isolation have been arranged in the barrel, I-beam support structure and concrete foundation.

The target chamber is a steel cylinder of 61 cm O.D. and 1.5 m length. Physical access and instrument ports are precisely machined in a horizontal plane and in planes 45° above horizontal.

Two sets of the ports are employed as X-ray windows and house the secondary spatial references. The references are cross wires with the separation distance between windows (nominally 30.0 cm) accurately determined by an optical comparator.

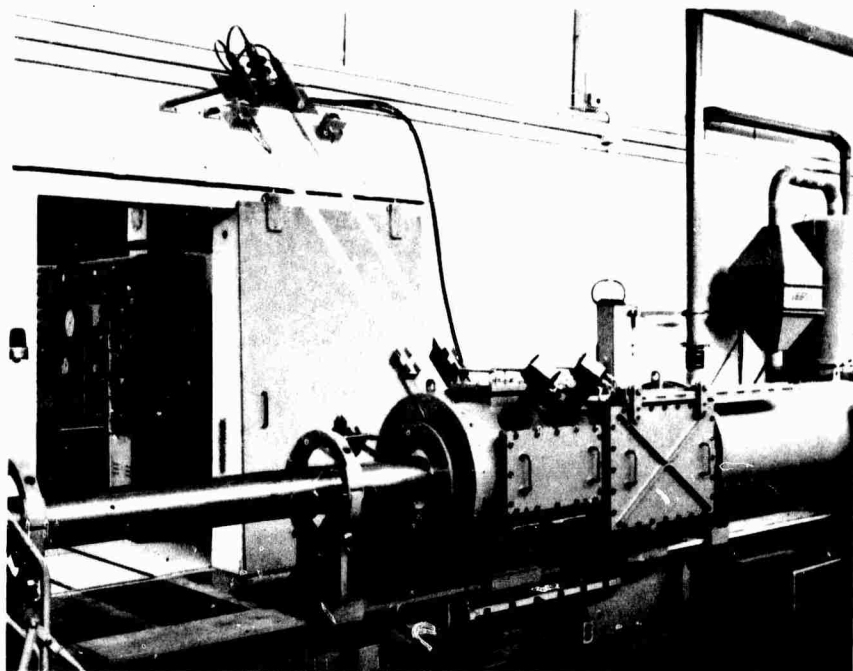


Figure 3 Target Chamber

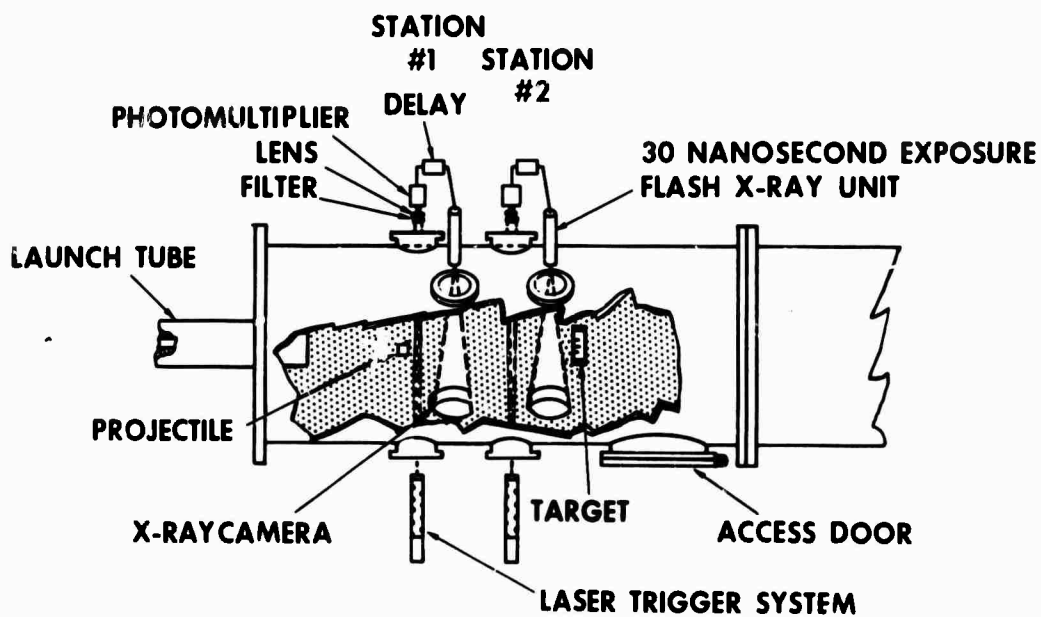


Figure 4 Top View of Target Chamber

MSL-70-01

Operationally, the ports are closed against O-ring vacuum seals with Plexiglas or magnesium windows for optical and X-ray instrumentation respectively or with steel cover plates.

INSTRUMENTATION

The impactor velocity measuring system consists of a two laser triggering system and a short duration dual flash X-ray developed by Lingle and Jones.⁽⁷⁾ With such a system, impactor velocities are measured accurately to $\sim 0.03\%$. The triggering system consists of two sets of neon-helium gas lasers aimed at photodetectors across the impact chamber orthogonal to and intersecting the line of flight of the projectile. Photomultipliers monitor the laser output through circular apertures and narrow band pass filters. When light interruption occurs at each station because of projectile passage, a sharp change of voltage level is converted into a trigger signal of sufficient voltage to initiate a Field Emission Corporation 30 nsec dual flash X-ray unit. The X-ray flash exposes a Polaroid film plate on the opposite side of the chamber by means of a fluorescing intensifier screen.

Spacing between the two X-ray field positions is indicated by fiducial wires which are measured by an optical comparator to within 0.1 mm. Measurements of the impactor face of the projectile relative to the window fiducials allow determination of the projectile position and distance traveled over the time interval measured between flash exposures.

Figure 5 is an example of the shadowgraphs taken at the two X-ray stations showing the projectile in free flight before impact.

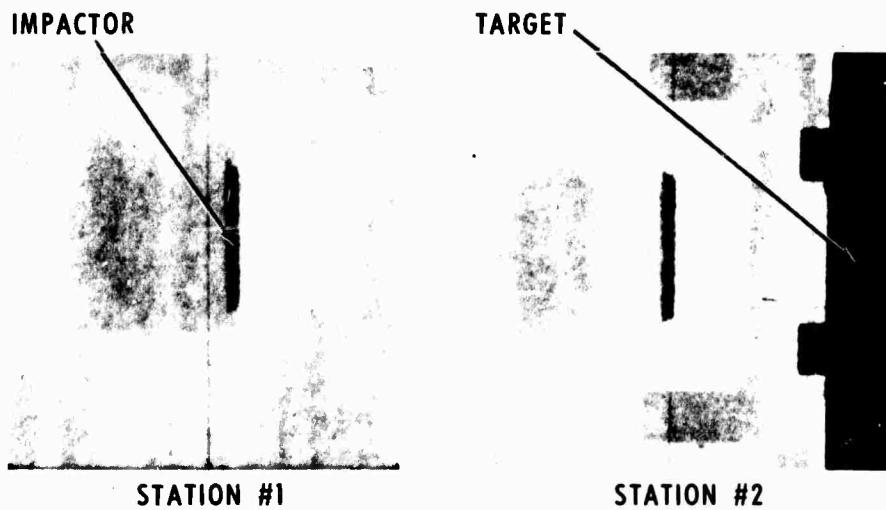


Figure 5 X-Ray Shadowgraphs of Projectile Before Impact

The free surface velocity data was collected through optical observation of the rear surface of the target blocks with a Beckman and Whitley Model 339B continuous-writing streak camera. This camera has the capability of recording at a rate of up to 9 mm/ μ sec on the film track. With the .076 mm wide slit normally used, the minimum time resolution is 10 nanoseconds.

For most of the experiments the camera was generally used only as a method of measuring time intervals and was not used to make any precise spatial measurements.

MSL-70-01

SECTION II

DESCRIPTION OF IMPACT EXPERIMENTS

Four methods were used to examine the arrival of rarefaction waves at the shock front: (1) Measurement of the motion of the surface as a function of time (laser velocity interferometer), (2) measurement of pressure as a function of time (manganin gage), (3) measurement of free surface velocity as a function of target thickness (step targets), and (4) measurement of shock velocity as a function of distance (optical wedge).

The majority of the experiments were conducted at the higher pressure levels using techniques (3) and (4). Design consideration of all four techniques are described below.

DESIGN OF EXPERIMENTS

The impactor plate had to be as thin as possible, posing problems in the design of projectiles capable of carrying undeformed plates to extremely high velocities. The initial design of these plates made provision for a reinforcing ring about the outside rear of the plate to provide stiffness. The plate thickness was one millimeter and the inside of the rear of the plate was supported by a thin plate of Zelux. It was found that this type of plate was very difficult to manufacture and finish so that the impactor front and rear surfaces were flat and parallel and that launch stresses caused severe plate curvature. The plate was redesigned such that it could be machined with uniform thickness. The sabot design

was also modified such that the plate was supported on a thick disc of Zelux. It was determined by impacting a mirror with such a plate and observing the mirror with the streak camera that the flyer plate was flat to within 0.05 mm causing less than 10 nanoseconds deviation.

The experiments were designed such that the wave was recorded before release waves from the corners and edges of the target arrived at the measurement position. Approximate shock relationships were established to provide reasonable design criteria.

The velocity of the head of the rarefactions was estimated to be:

$$c_e = 1.2 D + u_p \quad (2)$$

where c_e is the velocity of the elastic rarefactions and D is the shock velocity associated with the particle velocity u_p . The accuracy of this assumption is demonstrated in Figure 6 where release wave and shock velocities are compared for a variety of metals. This figure includes data from the present study as well as other sources. The tail of the rarefaction (return to zero pressure) was taken to travel at

$$c^2 = \frac{dP}{d\rho} \text{ taken at } P = 0 \quad (3)$$

where P is pressure and ρ is material density at pressure P .

LASER VELOCITY INTERFEROMETER

Experiments were performed at low stress levels using the laser velocity interferometer. This technique employs a He-Ne laser

MSL-70-01

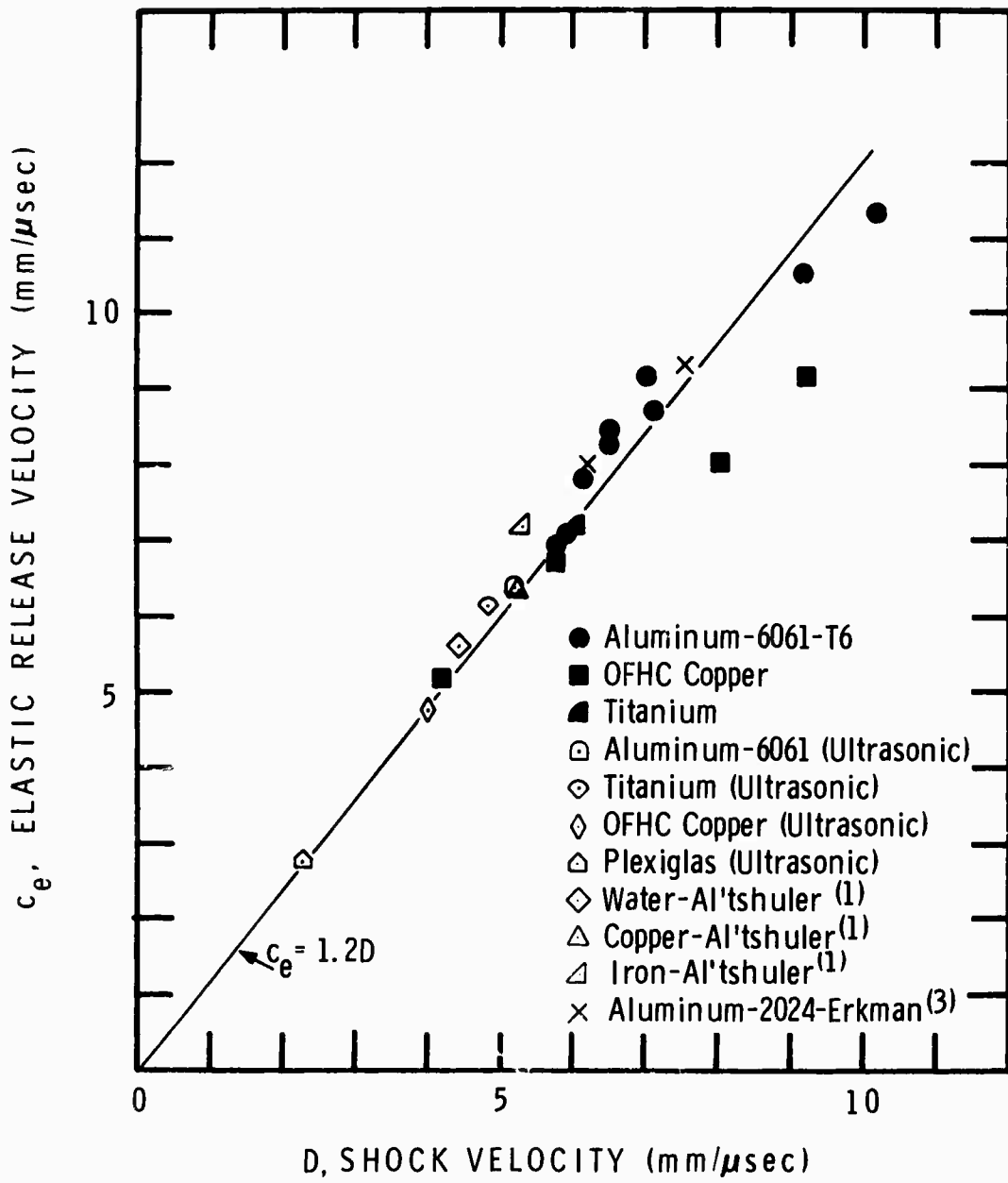


Figure 6 Elastic Release Wave Velocity vs Shock Velocity for Several Materials

to provide a monochromatic coherent light source. The beam from the laser is reflected from the rear surface of the target. This reflected beam is then split into two beams, one of which goes directly into a photomultiplier sensor while the second beam is delayed by reflection through a delay leg before recombination with the direct beam upon entry into the photomultiplier. Because part of the beam is delayed by the length of time required to traverse the delay leg, the beams upon recombination will show a phase relationship dependent upon the length of the direct and delay legs and the frequency of the two beams. For dynamic measurements the direct and delay leg path lengths will not change and changes in interference patterns are interpreted as changes in the frequency of the reflected laser beam. These frequency changes are due to changes in the velocity of the motion of the target rear surface. The laser velocity interferometer is therefore a doppler system.

The signal recorded shows no voltage change for constant velocities and (for uniform acceleration) sinusoidal variation of voltage for changes in velocity.

The data resulting from interferometer experiments consist of oscilloscope traces showing non-periodic voltage oscillations. These oscillations correspond to changes in the interference fringe pattern upon the photomultiplier sensor. Each full oscillation corresponds to one full fringe shift. From the fringe shifts the velocity of the surface can be found from

$$u = \frac{\lambda}{2\tau} \Delta N \quad (4)$$

MSL-70-01

where u is the velocity of the surface, λ is the wavelength of the laser light, τ is the time delay of the delay leg and ΔN is the total number of fringes recorded. Small changes in this calculation of velocity are necessary during portions of the wave in which changes in velocity take place in periods of time comparable to τ . In general the adjustment is made to the time at which a given velocity is recorded to account for the time the signal spends traveling through the delay leg. (In its simplest form this adjustment shifts the calculated times by $\sim \tau/2$).

The laser velocity interferometer allows very accurate velocity-time profiles to be obtained at low stresses. Because the stress wave being observed is reflected at the target rear surface, the wave interactions taking place may include spall. To record as much of the wave profile as possible, it is desirable to suppress spall. This may be accomplished by placing a transparent material of approximately the same impedance as the target on the rear surface and recording the motion of the interface. In this way a large part of the stress wave is passed through the target-window interface, thereby reducing the portion of the wave reflected as a tension wave and suppressing the tendency to spall. The amplitude of the reflected tension wave depends upon the impedance mismatch and on the initial amplitude of the compressive wave. Unfortunately, only a few transparent materials of limited impedance variation are available. This, and the fact that reflecting surfaces tend to degrade at higher pressure levels, generally limits the maximum pressure range for the interferometer technique to 100 to 200 kbars.

Using the previously discussed criteria, disk shaped targets were designed such that the area on the rear surface of the

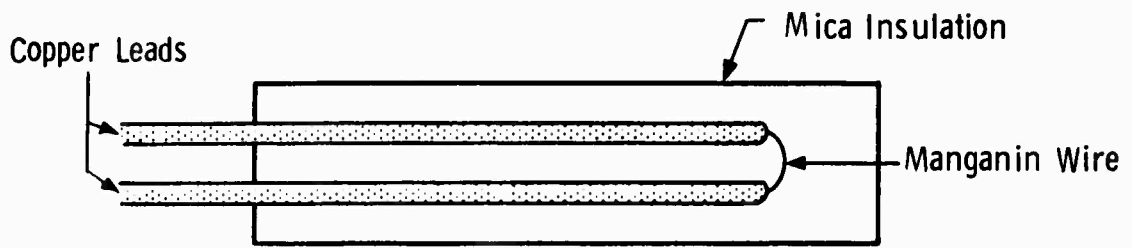
target used for reflection of the laser beam was unaffected by side rarefactions during the time of measurement. This design procedure was employed both for laser velocity interferometer and for manganin gage experiments, where the entire wave was recorded. Examination of records obtained with these instrumentation techniques have demonstrated that the target designs used were quite conservative.

MANGANIN WIRE GAGE

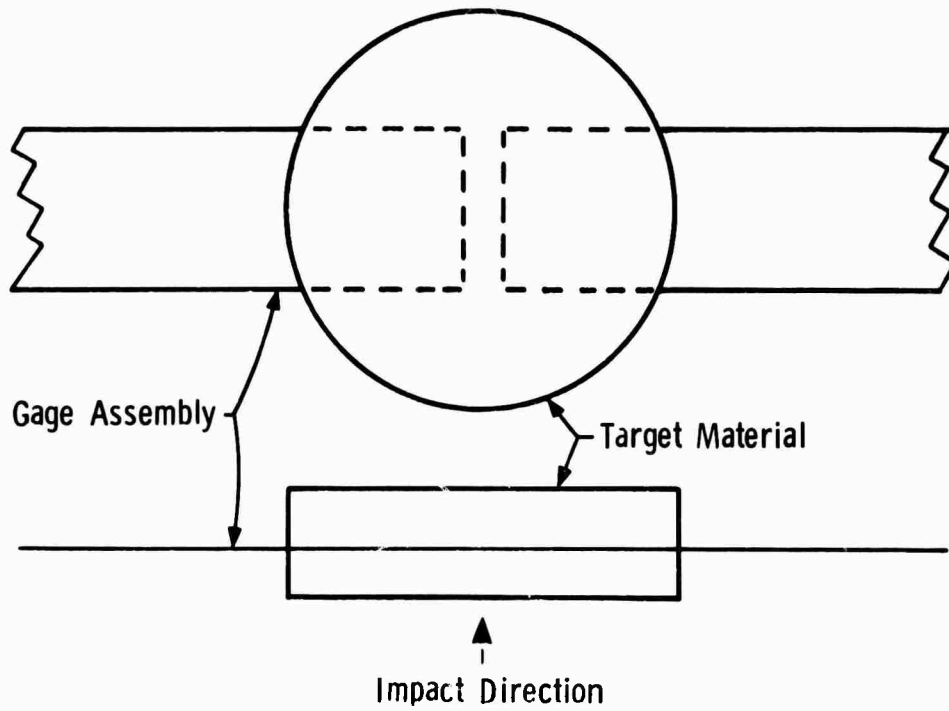
Experiments were performed with aluminum, copper and α titanium with manganin wire piezoresistive gages. These gages were developed and built by personnel of the Lawrence Radiation Laboratory. A description of the gage and its calibration can be found in Reference 8. The gages are constructed by plating copper on 0.025 mm diameter manganin wire, leaving about 7 mm of unplated wire as the active gage element. The gage element resistance is about 7 ohms. The plated leads are then flattened and the assembly placed between two thin (.025 mm) sheets of mica for electrical insulation. Total thickness of the assembled gage is about 0.15 mm. A sketch of such a gage assembly is shown in Figure 7. In the lower portion of the figure is shown the installation of the gage in a target. Each target was equipped with two gages to provide redundant measurements.

The manganin gage provides measurement of pressure as a function of time by means of the piezoresistive effect. The resistance of the gage is measured during the time the shock pressure pulse passes by the gage position. This is done by monitoring the voltage across the gage supplied by a constant current power supply. This supply provides a moderate voltage (tens of volts), high current (several amps) pulse to the gage for a

MSL-70-01



MANGANIN GAGE ASSEMBLY



MANGANIN GAGE TARGET

Figure 7 Manganin Wire Gage Construction

short period of time ($\sim 100 \mu\text{sec}$). By recording the voltage change and through time and resistance calibration the pressure-time history at the gage position may be determined.

The manganin wire gages were used at moderate pressures --- from about 76 kbars in aluminum and titanium to 400 kbars in copper. Attempts to use these gages at pressures higher than 400 kbars resulted in premature break-down of the gages.

The advantages of using the manganin wire technique are:

1. Ability to measure pressure time histories within the material being studied.
2. Capability to make measurements at higher pressure levels than are possible with quartz crystal and interferometer techniques.

The principal disadvantage is that the thickness of the gage and its different shock impedance than the surrounding material cause finite rise times which can obscure details of the stress wave profile. Also, the question of gage hysteresis (different, and possibly variable, piezoresistive coefficients on compression and release) has not been resolved with sufficient accuracy to determine the effect on experimental error.

STEPPED TARGETS

Because gages are not available to record stress-time or particle velocity-time at higher stress levels (> 400 kbars), it was necessary to employ a technique to observe free surface velocity at various depths in the target materials and from

MSL-70-01

these measurements infer release wave behavior. This was done by recording the time required for the surface to cross a known gap. The difficulty with this method is that if the shock that arrives at the free surface is attenuating, the surface may decelerate while crossing the gap. To avoid the timing error produced by this effect, a thin shim, preferably of the same material as the target, was applied to the rear surface. The situation of an attenuating shock in such a system is illustrated in Figure 8. A rarefaction wave is shown propagating with finite, discrete steps, represented by the characteristics AC, AE, etc., in the figure. After the attenuated compressive shock (OEB) reaches the rear surface of the shim and reflects as a rarefaction, the shim and target surface start to move together. When the shim-target interface is overtaken by the rarefaction wave (AC) the interface separates. The shim continues with the original free surface velocity while the surface itself is slowed to some lower velocity. Thus the shim indicates the free surface velocity associated with the peak particle velocity of the wave that struck the shim. If the shock wave was attenuated during its passage through the shim, the shim velocity will not correspond to the peak particle velocity but rather some lower average. In general, free surface velocity error with this technique will depend upon the shape of the wave. For a triangular wave of duration corresponding to the impactor-thickness (1 mm) and a shim of thickness 0.0125 mm, the error in the shim velocity would be 1.25%. This would seem to be representative of the worst case that would be encountered.

The basic target configuration was established as blocks with shims on the surface and measurement gaps for the shims to cross. The further side of the gap consisted of a mirror constructed by attaching aluminized Mylar to thick pieces of plate glass.

Only one side of the Mylar is aluminized and this surface was on the side opposite the side struck by the shim. This was done to avoid early extinction of the reflecting surface due to microjetting by the shim surface. Because of this thickness of film, the velocity measured was a combination of the shim velocity and the shock velocity in the Mylar due to the shim impact. A correction was made to determine the shim velocity using an estimate of the shock state in the Mylar. The magnitude of this correction can be estimated by calculating the shock velocity induced in the Mylar by assuming an impact of the shim material upon plexiglas. Using this approximation, it is calculated that the maximum correction on the measured velocity ranges from 0.03% at an impact velocity of 25 mm/ μ sec to 0.7% at a velocity of 7.3 mm/ μ sec.

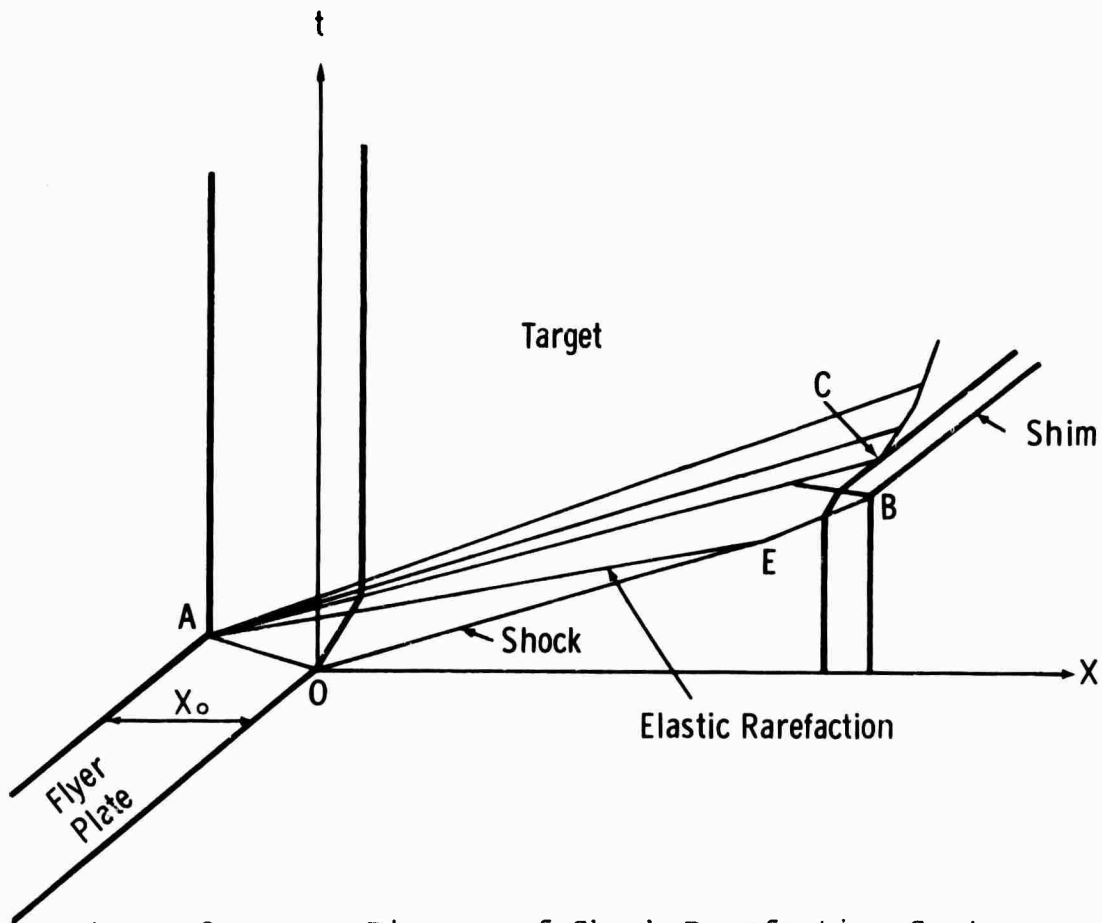


Figure 8 $x-t$ Diagram of Shock-Rarefaction System

MSL-70-01

The targets were designed with two or three different thicknesses in order to obtain as much information from each experiment as possible. The target design is shown in Figure 9. The target design allowed the same unaffected area on all steps for any target thickness.

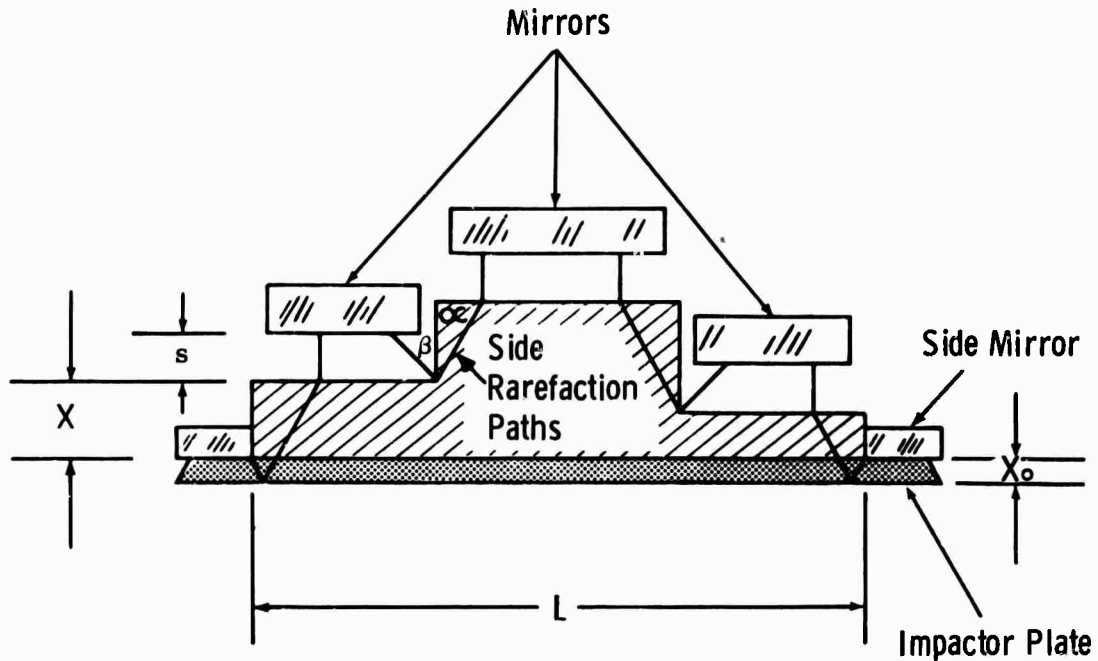


Figure 9 Step Target Design

The reflectance of the shim is decreased when struck by the shock wave indicating the start of the shim motion. The shim then crosses the gap and strikes the Mylar mirror. The mirror reflectance is also altered and the two changes in reflectance are measured on the streak camera record to provide the time of flight of the shim across the gap. A representative streak camera record is shown in Figure 10. Accuracies on the order of 0.5% to 2% in shim velocity are obtained when all errors are considered.

For attenuating shock waves, the particle velocity associated with the peak pressure was calculated from the measured surface

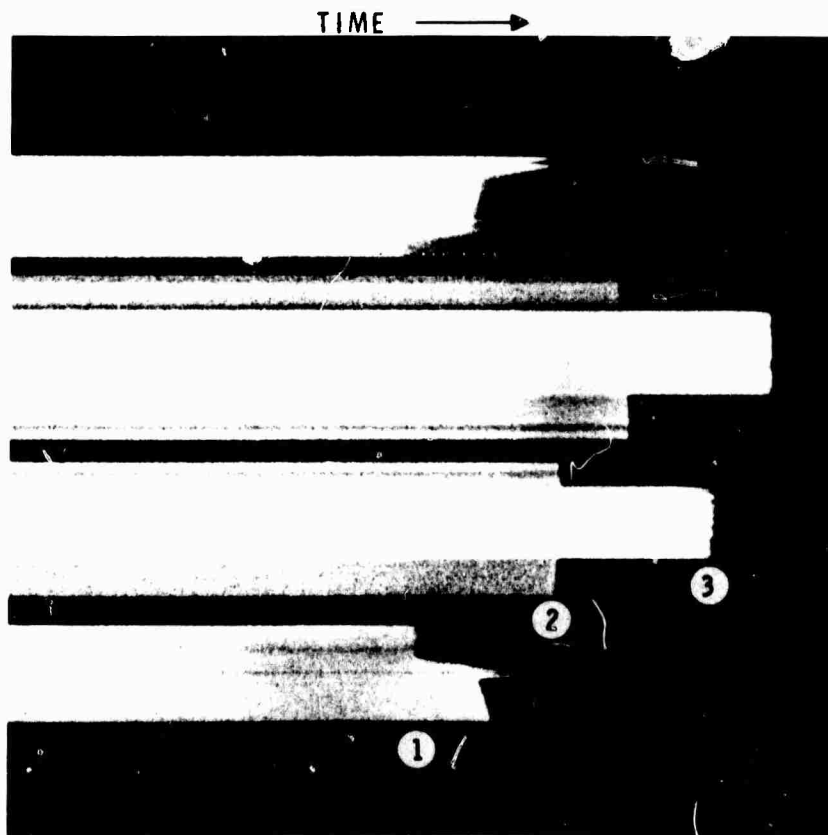
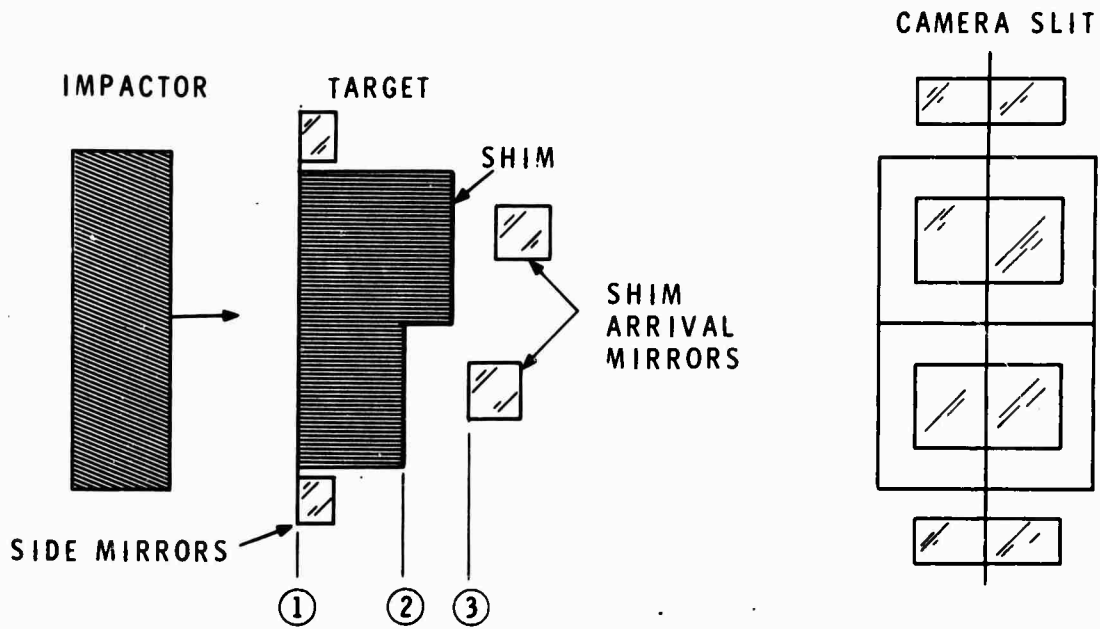


Figure 10 Step Target Technique

MSL-70-01

velocity. In several cases, the measured free surface velocity for unattenuated waves exceeded twice the known particle velocity. This effect is expected at high pressures as the irreversible entropy associated with the shock becomes appreciable. For copper this effect was noted at moderate pressures and became more evident at higher pressures. In aluminum, the effect was appreciable only for high velocity impacts. Figures 11 and 12 present the initial free surface velocity as a function of particle velocity (half the impact velocity for similar materials impacts) for the copper and aluminum respectively. Also included in the figures are the computed free surface velocities. These were calculated from:

$$u_{fs} = u_o + \int_{V_H}^{V_1} \left(\frac{-\partial P}{\partial V} \right)^{1/2} dV \quad (5)$$

assuming a Mie-Gruneisen equation of state and taking (γ/V) to be a constant.

Where: u_{fs} is the free surface velocity
 u_o is the particle velocity
 P is the pressure
 V is the volume
 H refers to the hugoniot
 S refers to the entropy.

As can be seen, the data is in good agreement with the computed values. From this it is possible to determine the particle velocity associated with a measured free surface velocity and to calculate the peak pressure in the attenuated shock as a function of distance of propagation.

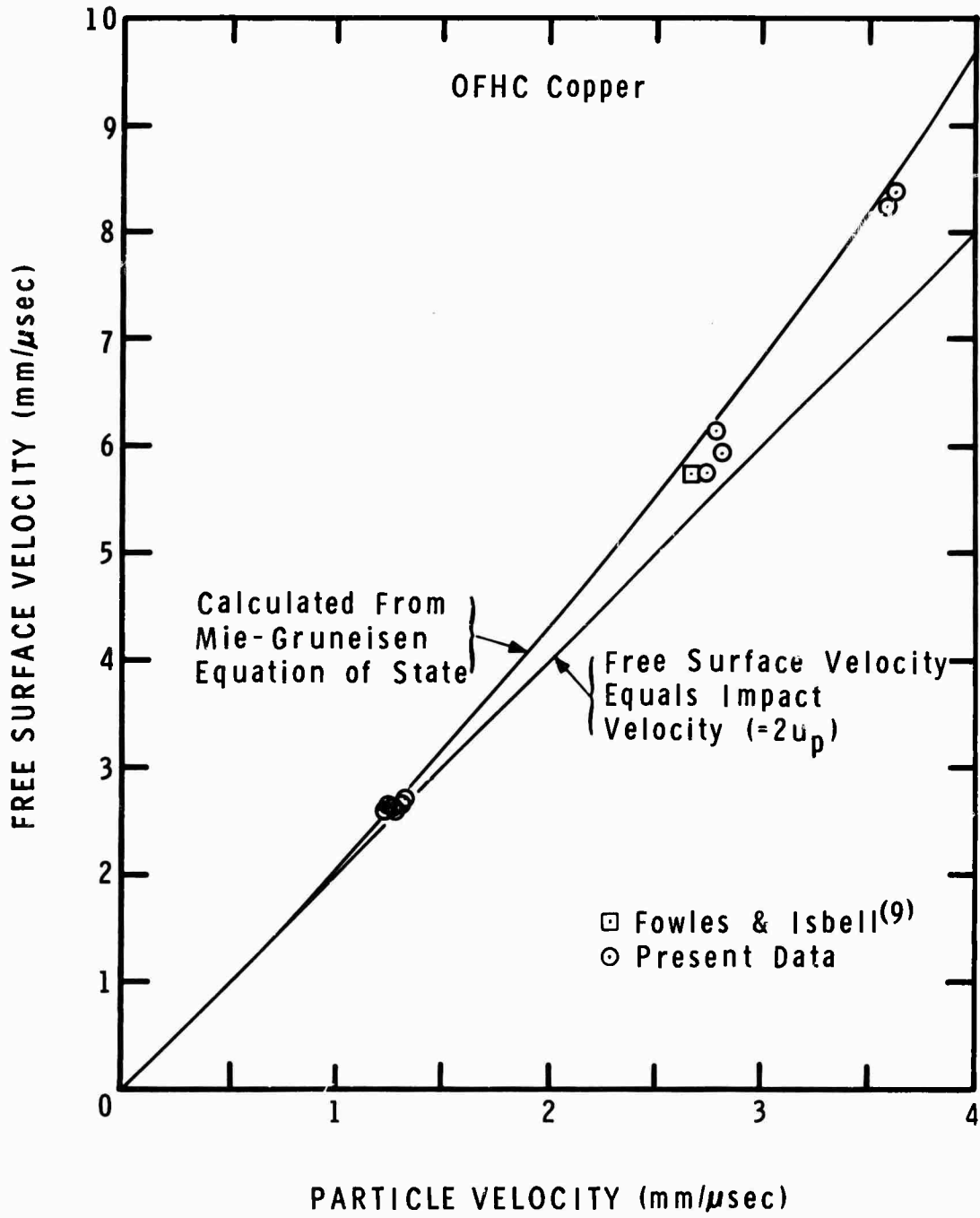


Figure 11 Free Surface Velocity vs Particle Velocity for Copper

MSL-70-01

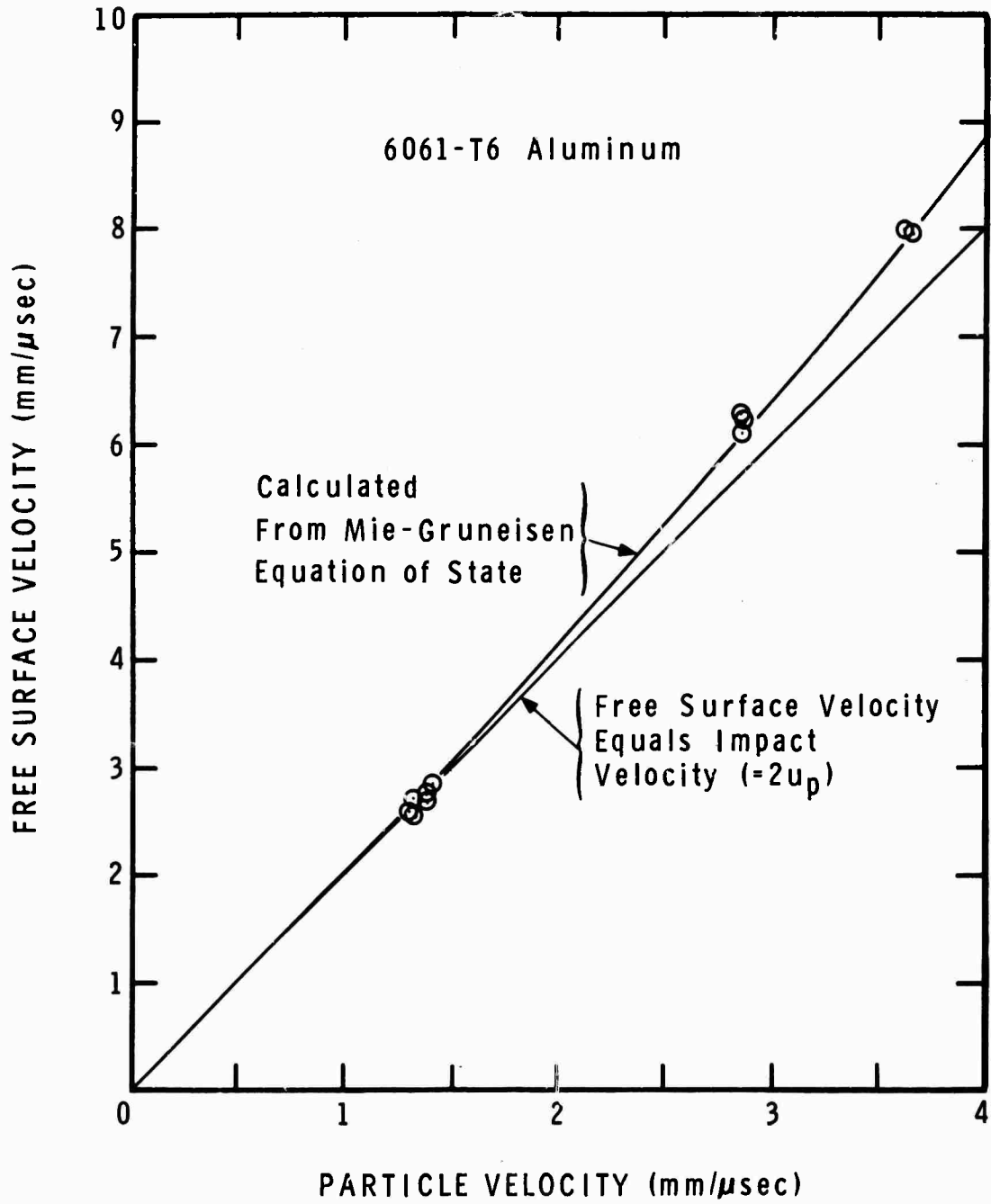


Figure 12 Free Surface Velocity vs Particle Velocity for Aluminum

The free surface shim technique allows determination of the particle velocity as a function of distance, at stress levels at which pressure or particle velocity gages will not function. The principle disadvantage to the technique is the fact that data is taken in increments and several experiments are required to characterize a particular condition. Also, at high pressures the errors in measurement may be sufficient to obscure the detail of the release waves. Thus the technique is primarily applicable to measurement of the elastic release wave velocity and of the attenuation due to the release wave.

WEDGE TARGETS

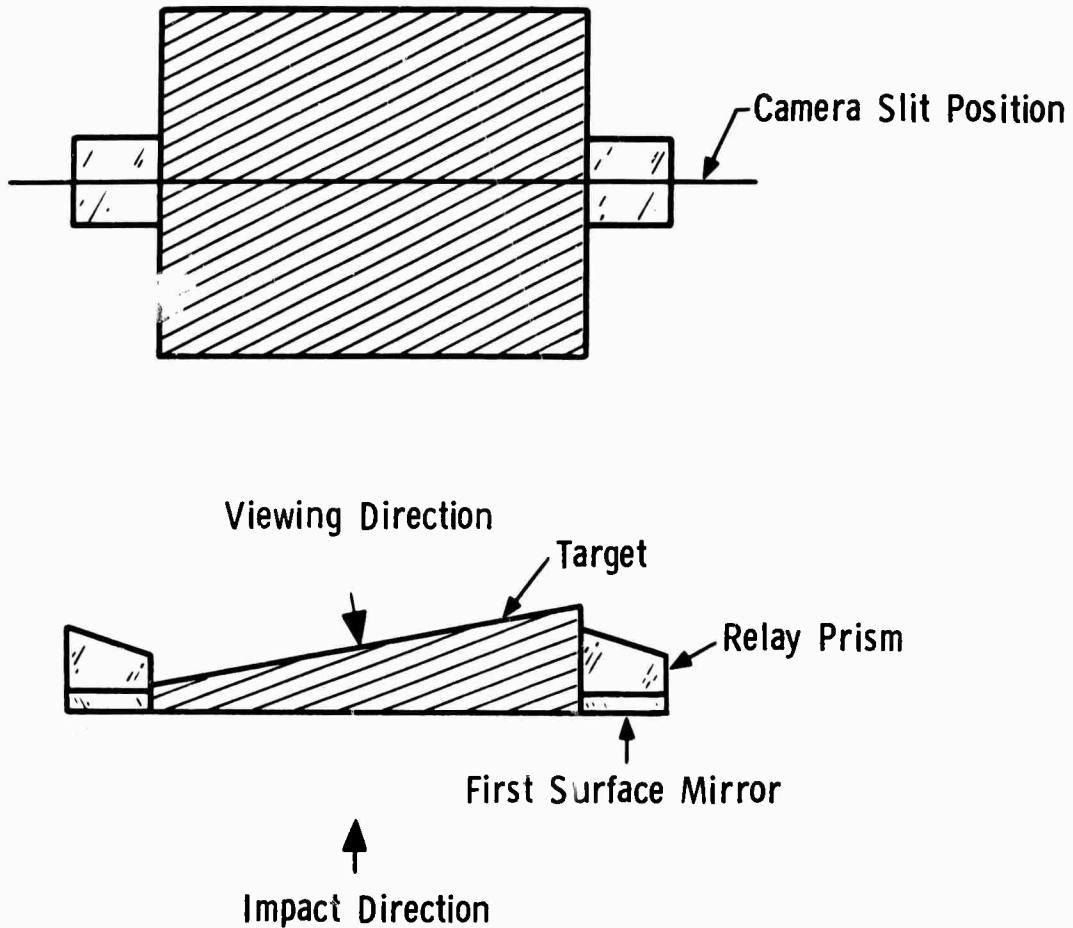
A few experiments at moderate pressures were performed with targets in the form of wedges. The purpose of these experiments was to examine continuously shock propagation versus distance in the material. The basic wedge configuration is shown in Figure 13.

The angle of the wedge was selected to insure inclusion of the overtaking point. The apparent velocity of the shock arrival along the wedge rear surface was greater than the velocity of the shock front in the material so that disturbances could not be communicated up the face of the wedge. The angles used ranged from 10° to 15° .

The first attempt to use the wedge was made using rear surface shims and a free surface gap to a mirror. This method was discarded because of unevenness of the record caused by small imperfections in the shim surface and the mirror.

Subsequent attempts to use wedges utilized direct observation of the target rear surface to record shock wave arrival.

MSL-70-01



WEDGE TARGET

Figure 13 Wedge Target Design

This is less desirable than observing free surface velocity because shock wave velocity is less sensitive to changes in the pressure of the attenuating wave than are the free surface or particle velocity. Figure 14 provides an example of a wedge record. The changes in shock velocity are evidenced by changes in the slope of the shock breakout.

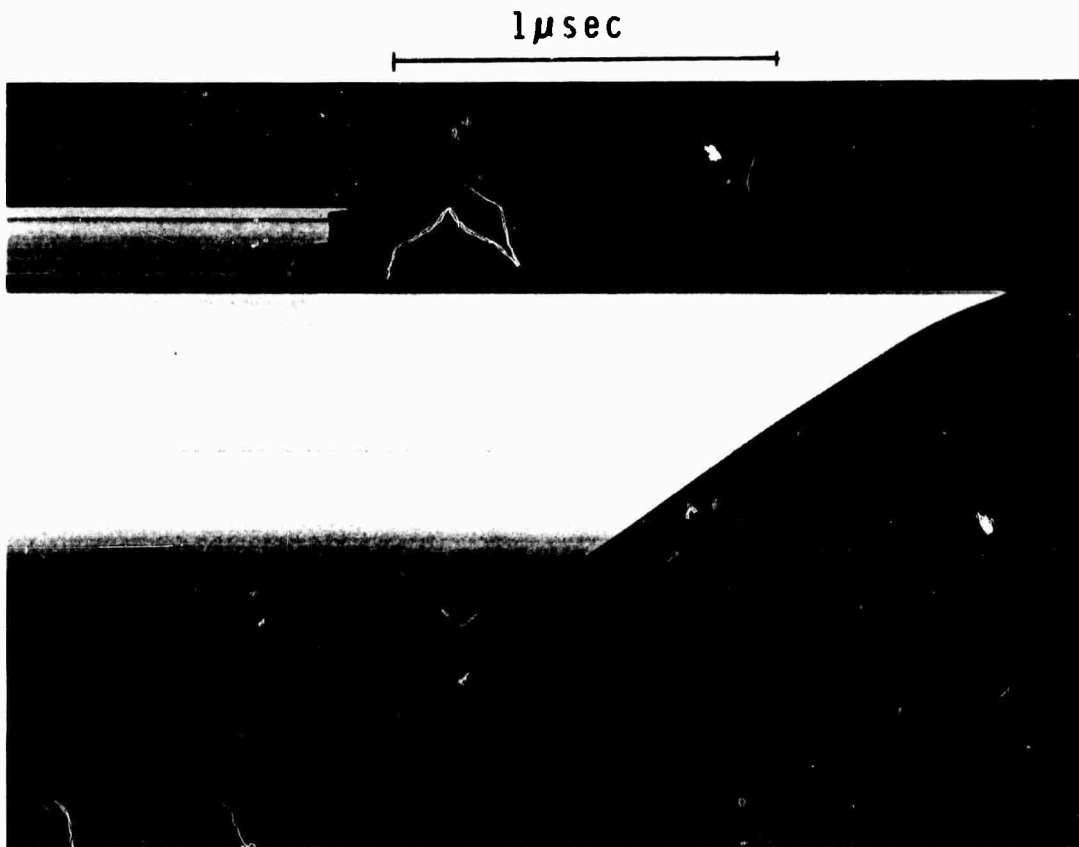


Figure 14 Wedge Streak Camera Record for
Copper-1.192 mm/μsec Impact Velocity,
Pulse Length 0.20 μsec

Because the attenuation information is in the form of small changes in slope extraction of data from records of this type is formidable task. Two methods have been used to process the data. The record was processed by converting the film record into a digital representation with an optical comparator (see Figure 15). The digital information was then processed in two ways. The entire shock arrival x-t path was fitted by a linear least squares fit for time as a function

MSL-70-01

of distance. Each point was then compared to this line and the difference plotted and recorded. This type of result is shown in Figure 16, the results from a copper record. The irregularity of this display is caused by point to point dispersion in reading the film record on the optical comparator and by the expanded time scale of the plot. The slope of the plot changes at between 22.5 and 25. This indicates the shock velocity decreased at this point, a normalized depth of $X/X_0 = 5.2$ to 5.6 . This decrease in shock velocity is interpreted as attenuation of the shock front by the release wave from the rear surface of the impactor.

The data was also analyzed by means of an "N" point differentiation scheme which calculates the local value of the derivative of distance along the face of the wedge with respect to time. The result of this processing is shown in Figure 17. As can be seen there is again a decrease in the derivative starting between 22.5 and 25 along the face of the wedge, in agreement with the least squares fit treatment. The derivative given on the plot is the velocity of the shock breakout across the face of the target, not the shock velocity in the material. Correcting for the wedge angle produces a shock velocity of $4.86 \text{ mm}/\mu\text{sec}$ for this experiment. This value is in good agreement with other copper measurements for the particle velocity of $0.596 \text{ mm}/\mu\text{sec}$.

Use of the wedge allows continuous observation of the shock wave front as it moves through the target material. In principle, this allows a very accurate determination of the point at which the shock front is overtaken by the first release wave. In practice the observed quantity, the shock velocity, changes so little with small changes in particle velocity, which are associated with the initial portion of the release wave, that the overtaking point is very difficult to determine.

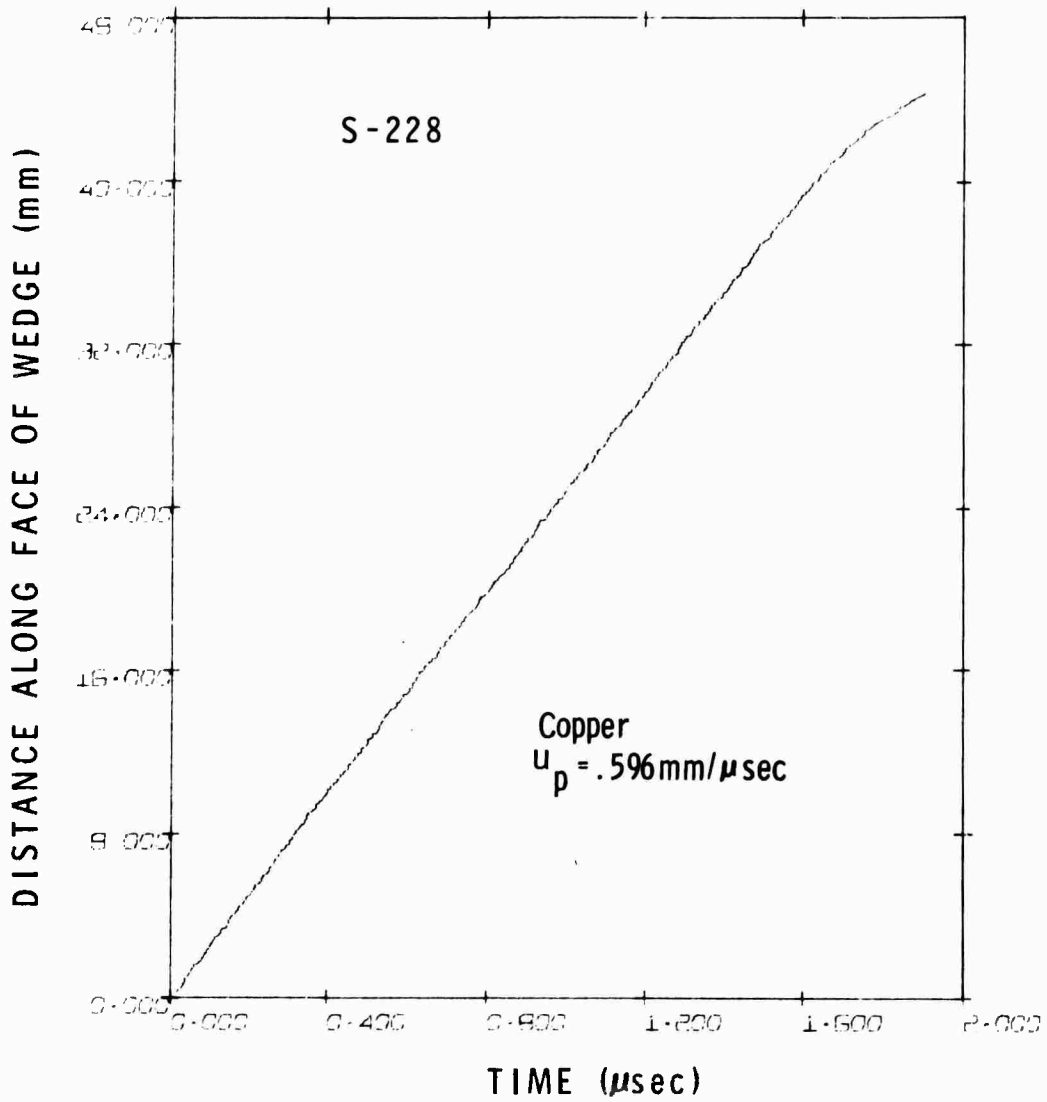


Figure 15 Distance-Time Record from Copper Wedge Record

MSL-70-01

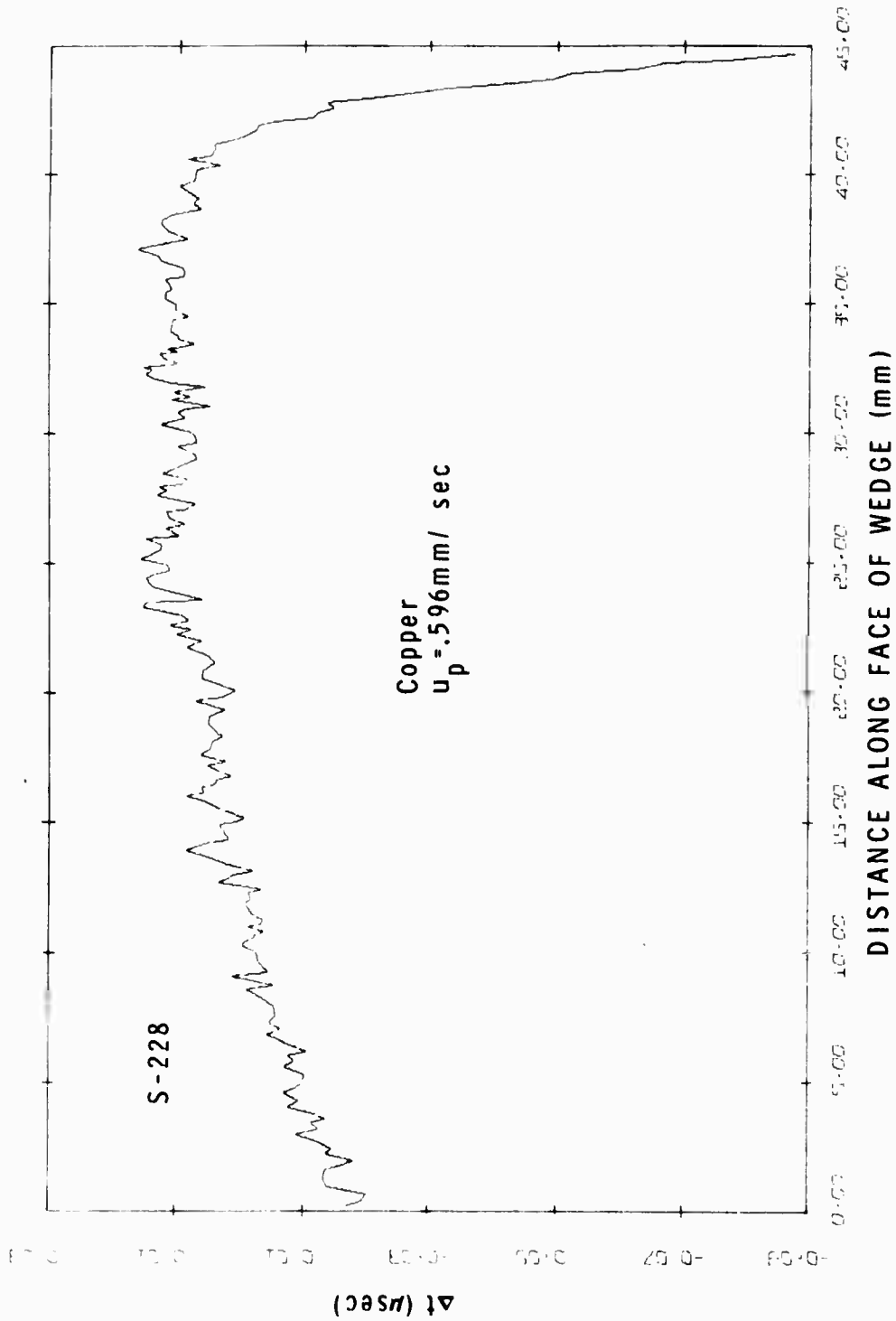


Figure 16 Delta Time vs Distance from Copper Wedge Record

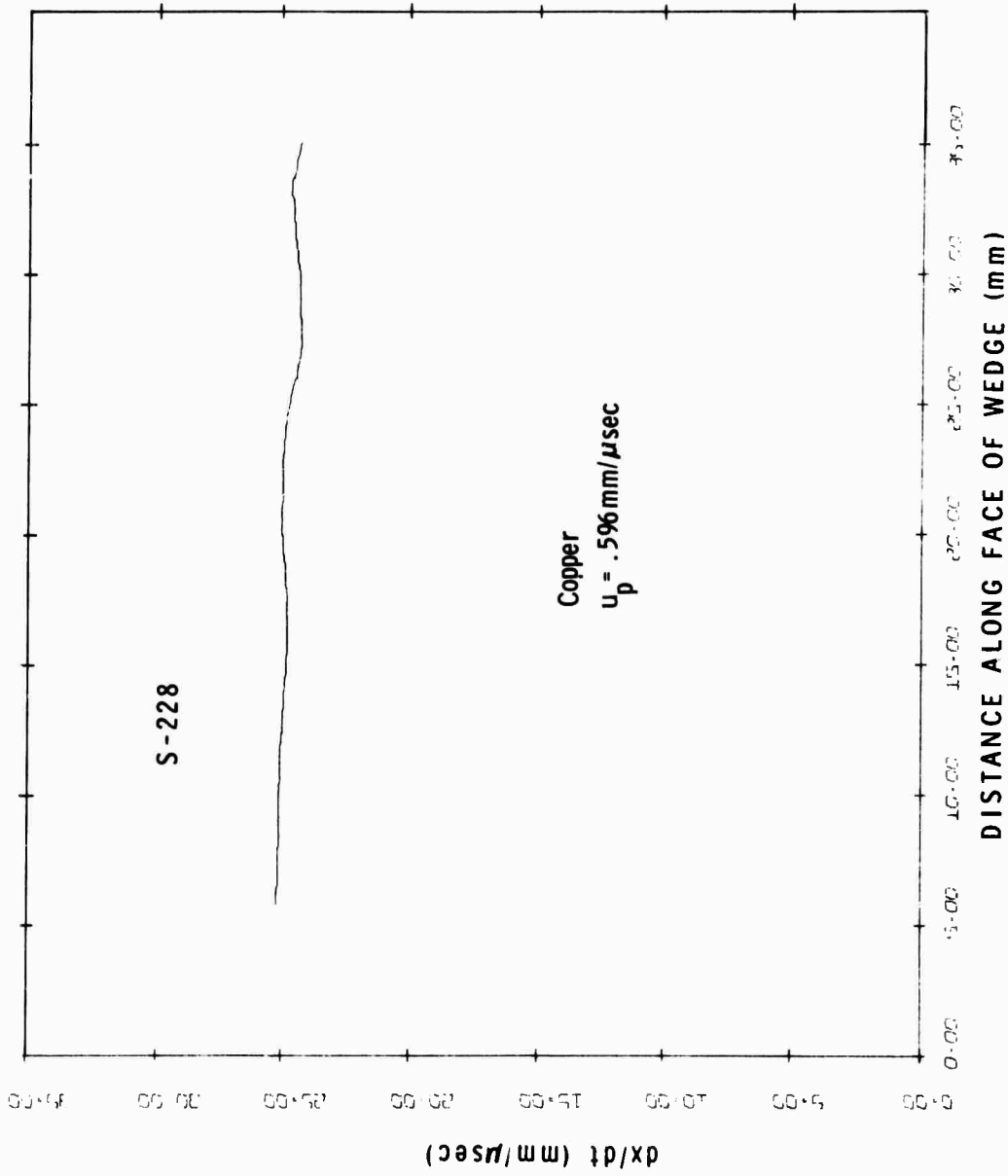


Figure 17 Velocity vs Distance from Copper Wedge Record

MSL-70-01

SECTION III

EXPERIMENTAL RESULTS

During the course of the program the following materials were examined experimentally:

1. OFHC Copper
2. 6061-T6 Aluminum
3. 6Al-4V Titanium
4. Pure Titanium (in the α phase)
5. S-200 Beryllium
6. A Beryllium supplied by Lawrence Radiation Laboratory similar to Brush Beryllium QMV
7. An Uranium Alloy

Table I presents the yield strengths, elastic properties and shock properties of these materials.

OFHC COPPER

This pure (.999) form of copper has a relatively low yield (2.7 kbar compressive yield strength), is ductile and strain rate sensitive. Experiments performed at low pressures (52 kbars) were instrumented with the laser velocity interferometer. These profiles are presented in Figure 18 in terms of interface velocity versus time. In order to suppress spall such that the unloading portion of the wave could be observed,

TABLE I

	COMPRESSIVE						HUGONIOT		
	P_0 gm/cm ³	Yield (kbars) 10 ⁻³ /sec	C_1 mm/usec	C_g mm/usec	C_0 mm/usec	v	Y_0	Linear Fit C_2 (mm/usec)	S
6061-T6 Aluminum	2.70	3.2 (10)	6.368 (11)	3.197 (11)	5.19 (11)	.331 (11)	2.00 (14)	5.326 (14)	1.338 (14)
OFHC Copper	8.92	2.7 (11)	4.757 (11)	2.247 (11)	3.99 (11)	.356 (11)	1.99 (14)	3.94 (14)	1.489 (14)
6Al-4V Titanium	4.50	9.6*	---	---	---	---	1.09 (14)	4.695 (15)	1.146 (15)
Titanium α -Phase	4.50	5.1 (11)	6.118 (11)	3.246 (11)	4.83 (11)	.304 (11)	1.09 (14)	4.695 (14)	1.146 (14)
S-200 Beryllium	1.85	2.3 (12)	12.196	8.86	7.87	.005	1.16 (14)	7.998 (14)	1.124 (14)
OMV Beryllium	1.85	2.71 (13)	---	---	---	---	1.16 (14)	7.998 (14)	1.124 (14)
Uranium Alloy	16.41	---	---	---	---	---	---	2.92 (16)	0.63 (16)
								for $u < .5$ mm/usec	
								2.57 (16)	1.50 (16)
								for $u < .5$ mm/usec	

*Manufacturer's Specifications

MSL-70-01

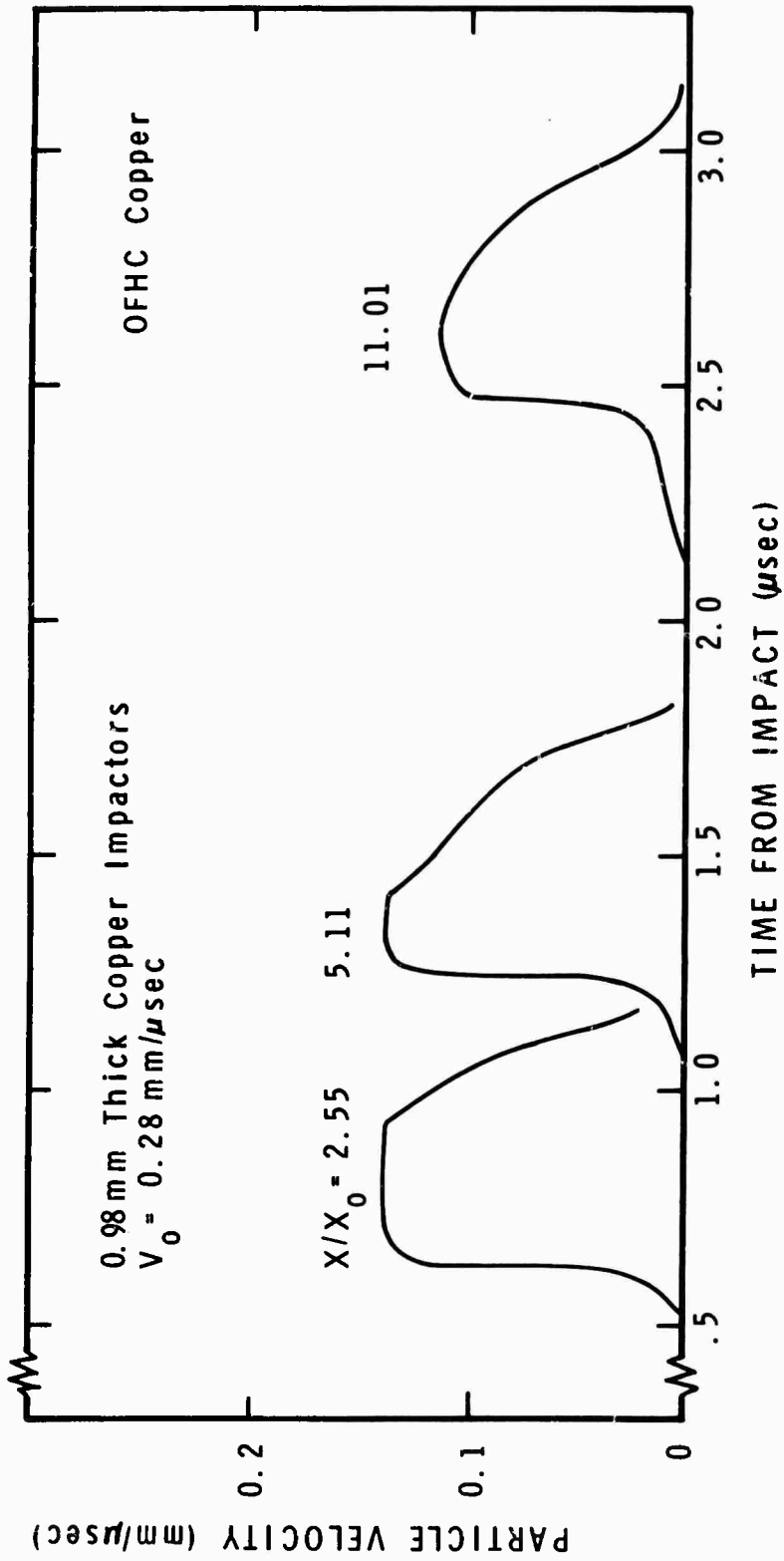


Figure 18 Copper Interferometer Records

the experiments were performed with fused quartz windows on the target rear surfaces. The laser beam was reflected from the quartz-copper interface. Due to the impedance mismatch between the target and window the interface velocity is greater than the particle velocity, but is less than the free surface velocity. Profiles were obtained for three values of X/X_0 (target thickness/impactor thickness); 2.55, 5.11 and 11.01.

In all the profiles a ramped elastic precursor is evident with a velocity of 4.75 mm/ μ sec followed by a ramped plastic wave with a velocity of \sim 4.5 mm/ μ sec. There is no definite elastic-plastic release wave structure evident in these profiles. The indicated release wave velocity of greater than 5.3 mm/ μ sec exceeds the expected plastic release wave velocity. Although there is no clear cut elastic-plastic release wave structure, the first release wave, because of its velocity evidently is an elastic wave.

A number of intermediate pressure experiments were performed at about 400 kbars with manganin wire gages. Typical of the results of these experiments is the pressure-time profile shown in Figure 19. The elastic precursor is not observed at this pressure level as the shock is overdriven (the shock velocity is greater than the elastic precursor velocity). There is a finite rise time on the front of the wave that is attributable to impact tilt and to the finite gage thickness. There is also some unevenness on the top of the record due to system noise. The smeared elastic-plastic nature of the release wave can be seen in this record with an initial drop in pressure followed by a change in slope and then another pressure drop. The double inflection is taken to be the demarcation between elastic and plastic behavior. The stress does not return to zero because the copper impactor plate was backed

MSL-70-01

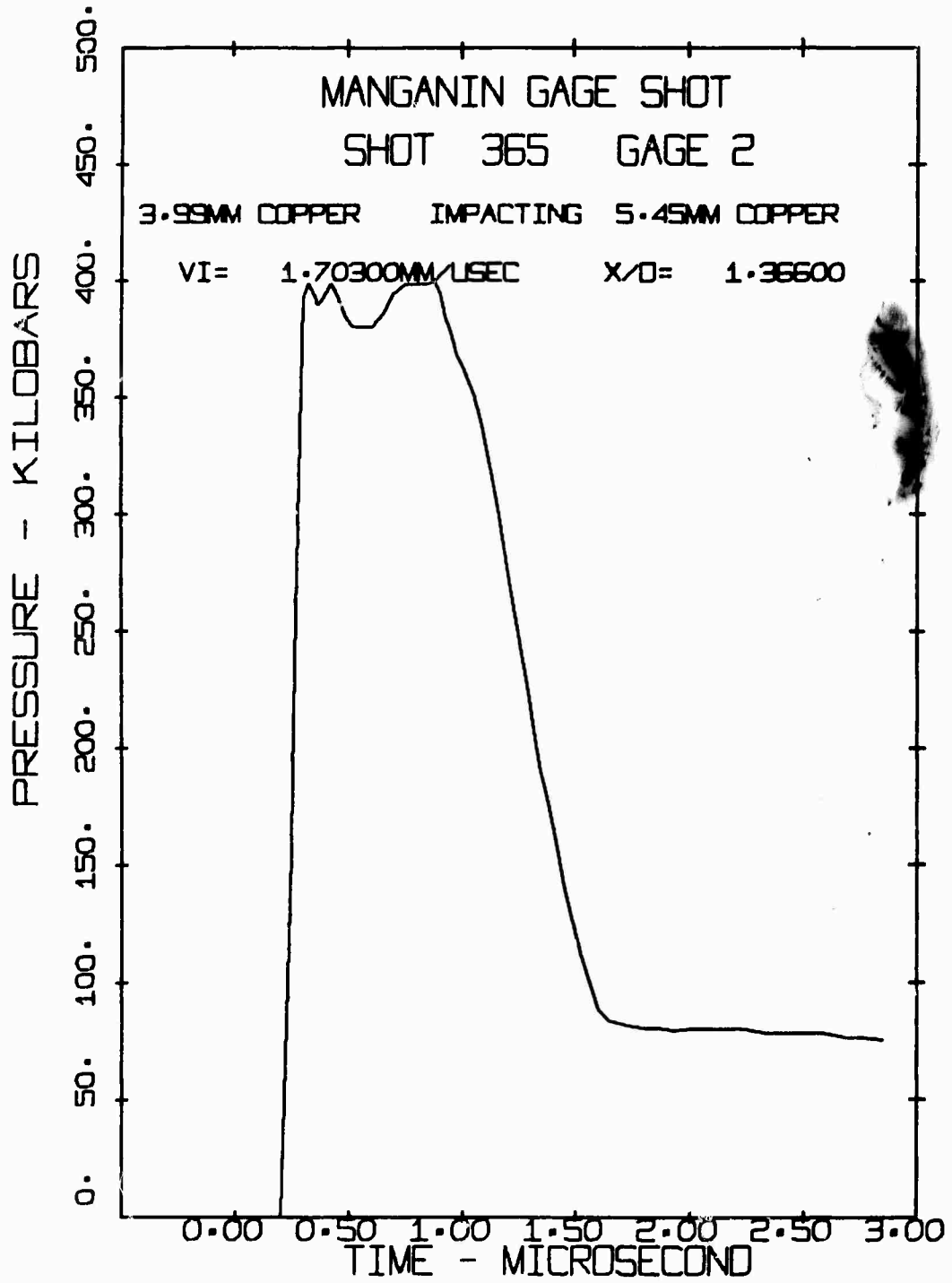


Figure 19 Copper Manganin Wire Record

with a plastic plate to insure impactor flatness. Again examination of the velocity of the first release wave shows it to be much higher than expected for the plastic release wave.

In order to obtain comparisons of the pressure-time records with other forms of data the manganin records were transformed through the conservation equations:

$$d\rho = dP/c^2 \quad (6)$$

and

$$du = dP/\rho c \quad (7)$$

where ρ is the local material density

P is the pressure

c is the local sound speed

u is the particle velocity.

The results could then be transformed into the particle velocity or free surface velocity versus distance plane through the method of characteristics as shown in Figure 20. The elastic-plastic nature of the release wave is no longer evident. The same procedure was used to project the pressure-time results into the stress-strain plane. In Figure 21 the result of this transformation is shown along with the huginot of the material. The loading path here is taken along a Raleigh line. The unloading path drops below the huginot indicating elastic release. The release path cannot be followed to zero stress because of the plastic backing of the impactor plate. This experimentally determined stress-strain release path shows no definite change from elastic to plastic behavior. If the

MSL-70-01

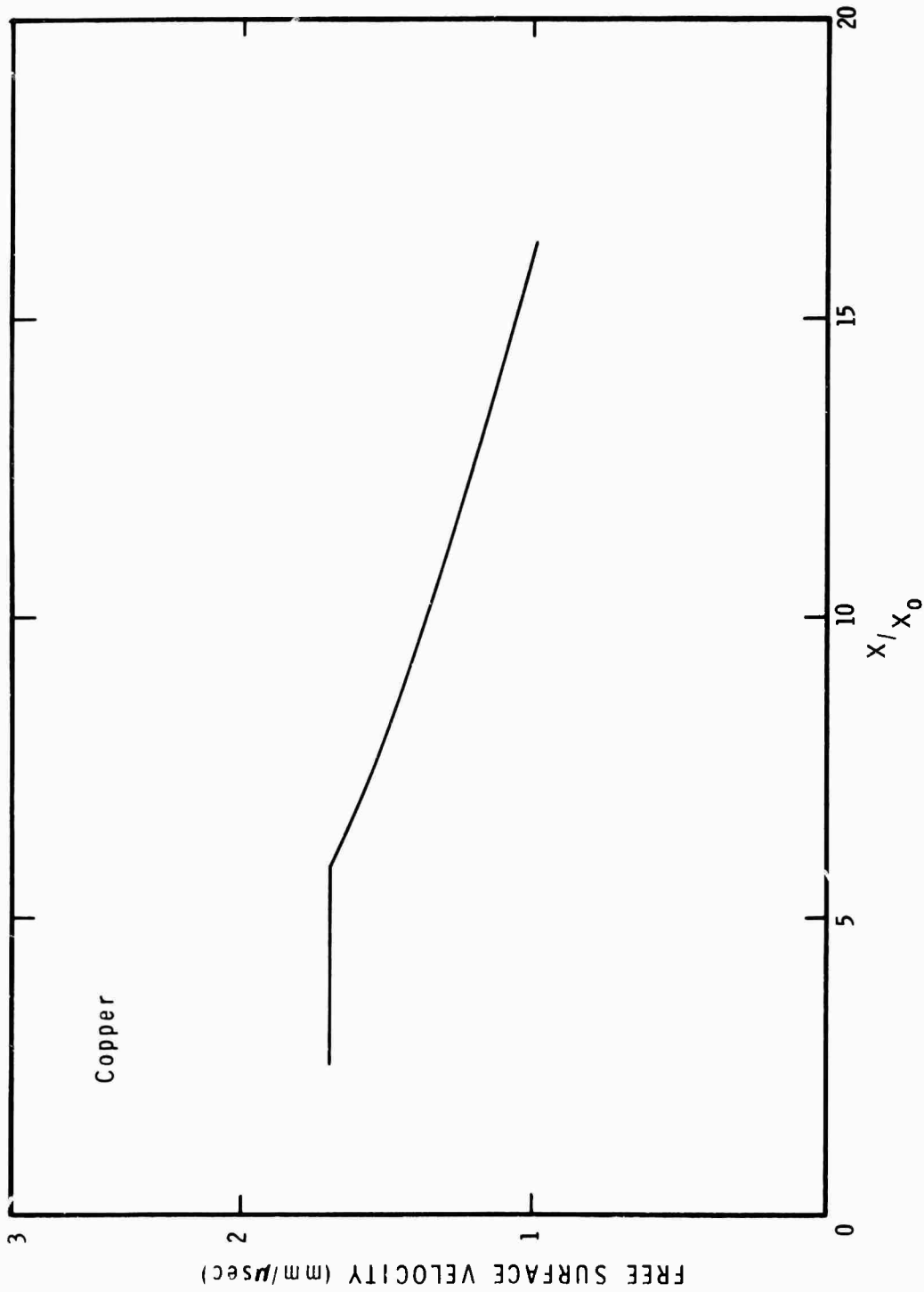


Figure 20 Free Surface Velocity vs Distance for Copper from Manganin Wire Gage Record

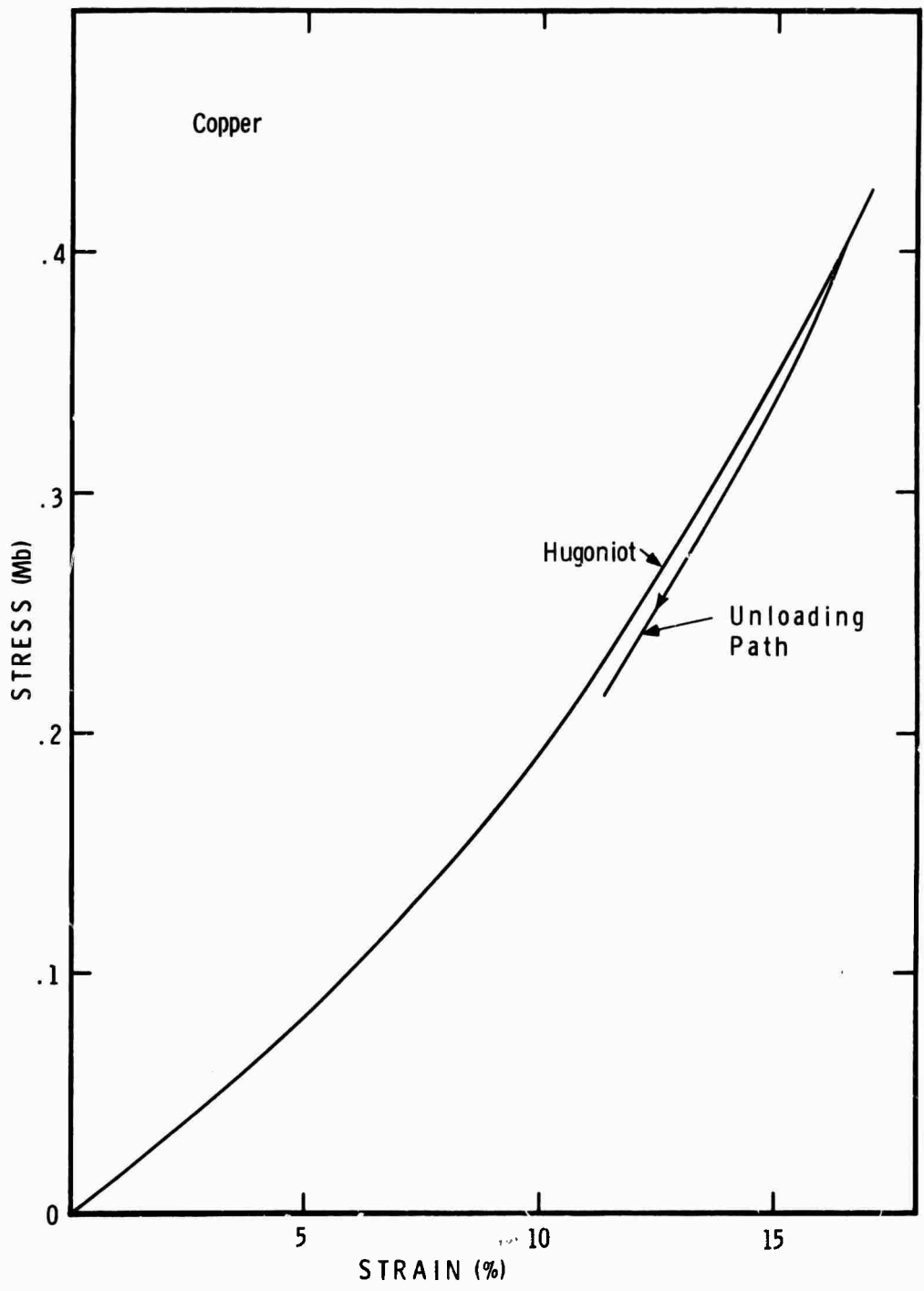


Figure 21 Copper Stress-Strain Release Paths from Manganin Wire Gage Records

MSL-70-01

maximum difference in stress between the hughoniot and the release path is taken to be 4/3 of the yield, the value of the yield strength is then about 10 kbars at 400 kbars peak pressure from these experiments. This is to be compared with the quasi-static yield of 2.7 kbars and the value of 3.2 kbars yield at 10^3 /sec strain rate.

Attempts to obtain pressure-time profiles at higher stress levels were not successful due to premature gage failures. Data at higher pressures was obtained through the free surface technique. Experiments were performed at impact velocities of 2.5, 5.6 and 7.3 mm/ μ sec corresponding to pressures of 0.65, 2.01 and 3.03 Mbars. Data from experiments at an impact velocity of 2.5 mm/ μ sec are shown in Figure 22. The overtaking point is clearly between values of X/X_0 of 4.5 and 5.5. Also shown in this figure is the overtaking point determined from a wedge experiment. The overtaking point from the two types of experiments agree quite well.

Results from experiments performed at an impact velocity of 7.3 mm/ μ sec are shown in Figure 23. Here because of irreversible heating effects, the free surface velocity was significantly higher than the impact velocity. The overtaking point lies between X/X_0 of 4 and 4.4 indicating a release wave velocity between 8.91 and 9.48 mm/ μ sec. Because of the large amount of heating at the peak pressure level, the free surface velocities cannot be taken to be twice the particle velocities. The values must instead be corrected for heating effects through Equation 5.

The normalized attenuation for initially unattenuated pressures of 0.4, 0.65 and 3.03 Mbars are presented in Figure 24. With increasing pressure the distance before initial attenuation

MSL-70-01

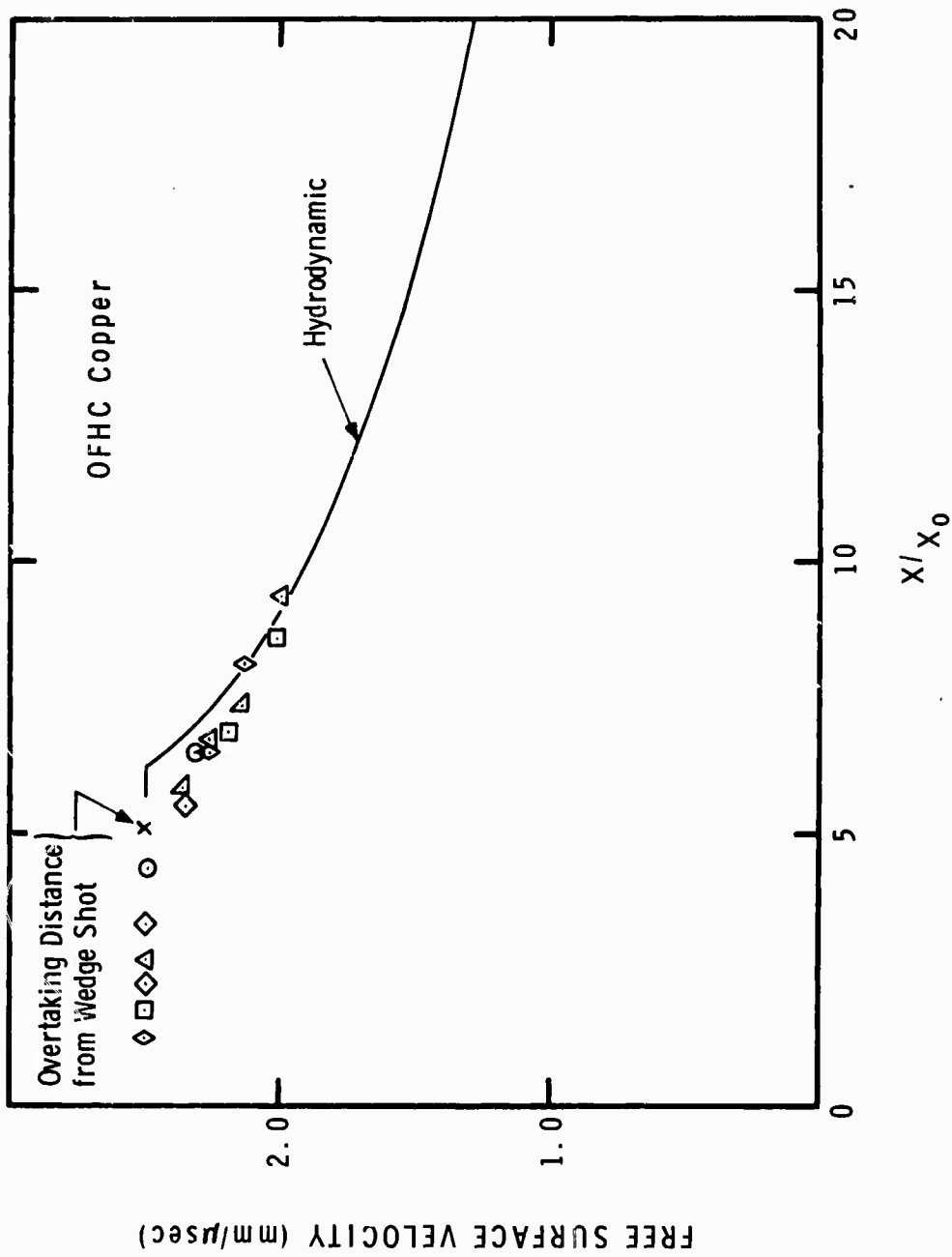


Figure 22 Free Surface Velocity vs Distance for Copper-2.5 mm/μsec Impact Velocity, Normalized to Ufs=2.5 mm/μsec at X/X₀=2, Pulse Length 0.17 μsec

MSL-70-01

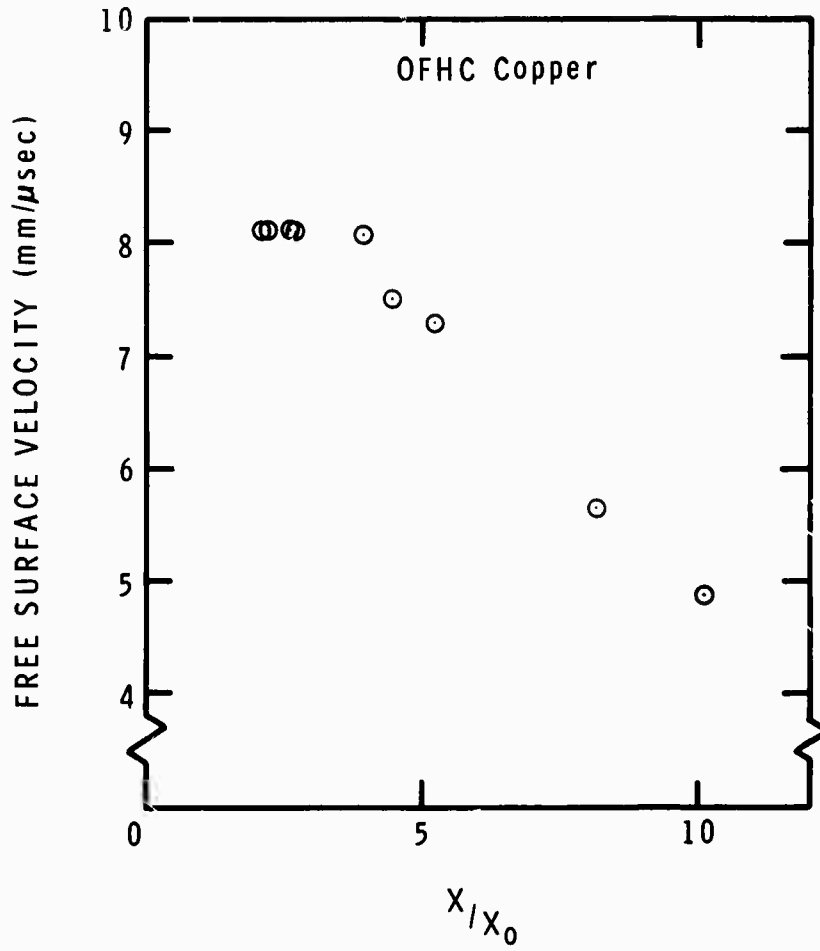


Figure 23 Free Surface Velocity vs Distance for Copper-7.3 mm/ μ sec Impact Velocity, Normalized to $U_{fs}=8.2$ mm/ μ sec at $X/X_0=2$, Pulse Length 0.16 μ sec

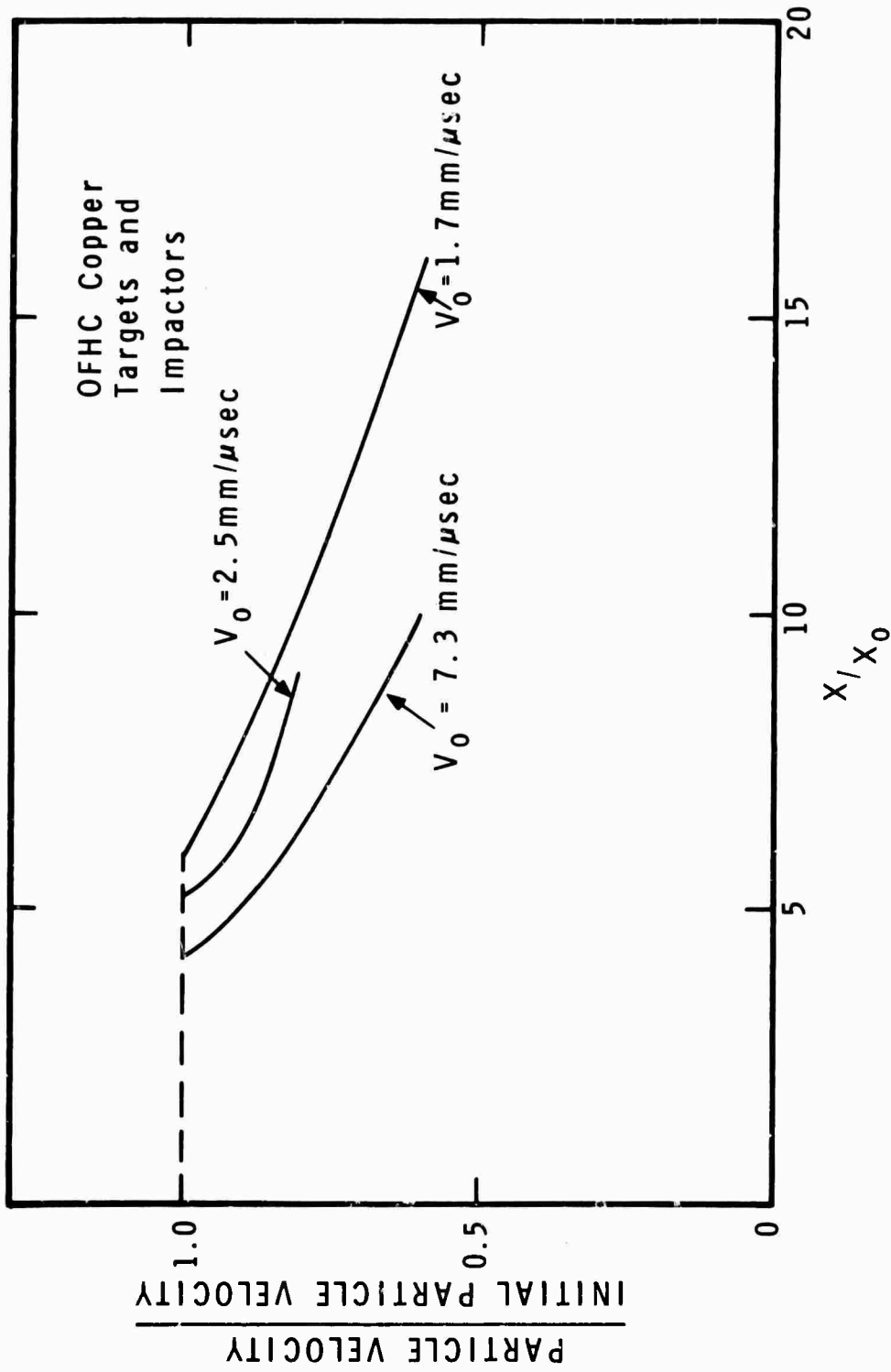


Figure 24 Normalized Attenuation for Copper

MSL-70-01

takes place becomes less and the initial rate of attenuation increases. The initial release wave velocities inferred from the experimental results are presented in Figure 25 as a function of ρ/ρ_0 or relative compression. The plastic release wave velocities as determined by Al'tshuler, et al.⁽¹⁾ are also shown along the calculated hydrodynamic release wave velocities. The calculated release wave velocities are obtained using the Mie-Gruneisen equation of state the linear fit to the hogniot resulting in:

$$c^2 = v^2 \left[\frac{\gamma P}{V} \left(1 - \frac{1}{1-Sn} \right) + \rho_0^2 c_0^2 \frac{1+Sn}{(1-3n)^3} \right] \quad (8)$$

where V is the specific volume behind the shock

P is the shock pressure

c_0 and S are the constants of the linear fit of shock velocity, D , to the particle velocity, u , $D = c_0 + Su$

γ is the Gruneisen parameter and

$$n = 1 - \frac{V}{V_0}$$

The sound velocities were calculated assuming γ/V is a constant.

The value shown on the ordinate of Figure 25 is the longitudinal wave velocity determined from ultrasonics measurements.

The initial release wave velocities determined from the lower pressure experiments agree well with the elastic release wave velocity for copper given by Al'tshuler et al.⁽¹⁾ The two

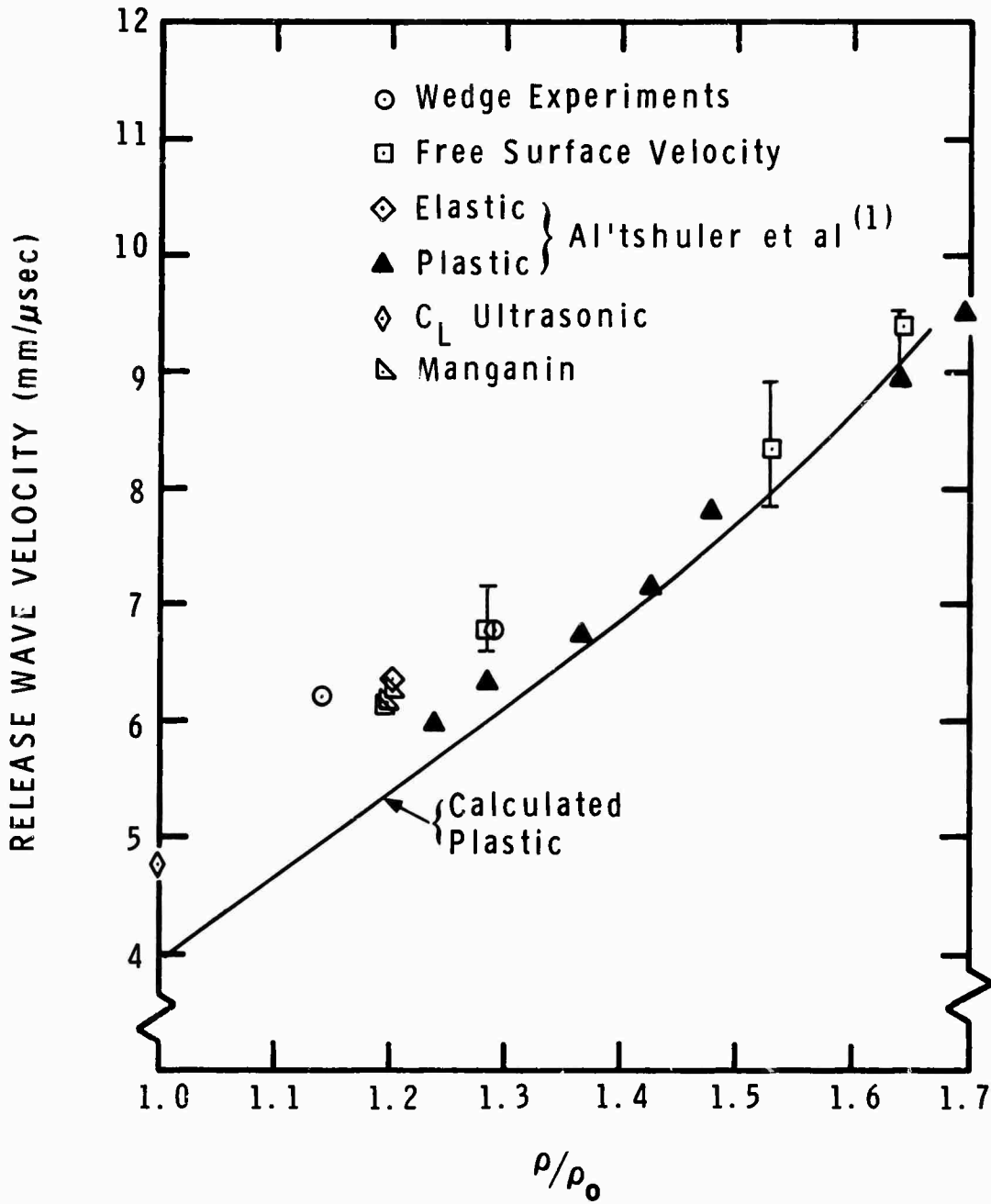


Figure 25 Release Wave Velocity vs Compression for Copper

MSL-70-01

highest pressure points agree, within the error shown, with the Al'tshuler plastic wave data points and the calculated plastic release wave velocity. These results are taken to show an approach to purely hydrodynamic behavior.

6061-T6 ALUMINUM

This alloy of aluminum is fairly strong with a compressive yield of about 3.2 kbars, ductile and strain rate insensitive at room temperature.

A series of intermediate pressure experiments were performed with manganin wire gages to examine the unloading of the aluminum alloy. The experiments resulted in the series of pressure-time profiles shown in Figure 26. The peak pressures here range from 76 kbars to 237 kbars. An elastic precursor is not observed at these pressure levels and the finite rise time is attributed to shock tilt across the gage and the finite gage thickness. As higher pressures are attained in the material the elastic-plastic structure of the unloading wave becomes more obvious. Although there is no elastic stress plateau the waves are reasonably clear. An increase in the magnitude of the elastic release wave can be observed with increasing pressure. In these records the release wave does not go to zero pressure because the impactor is backed with a plastic plate to insure flatness during launch.

Again, in order to obtain comparisons of the pressure-time records with other forms of data the manganin records were transformed through the conservation Equations 6 and 7.

When the manganin records of the aluminum experiments are projected onto the free surface velocity versus normalized target

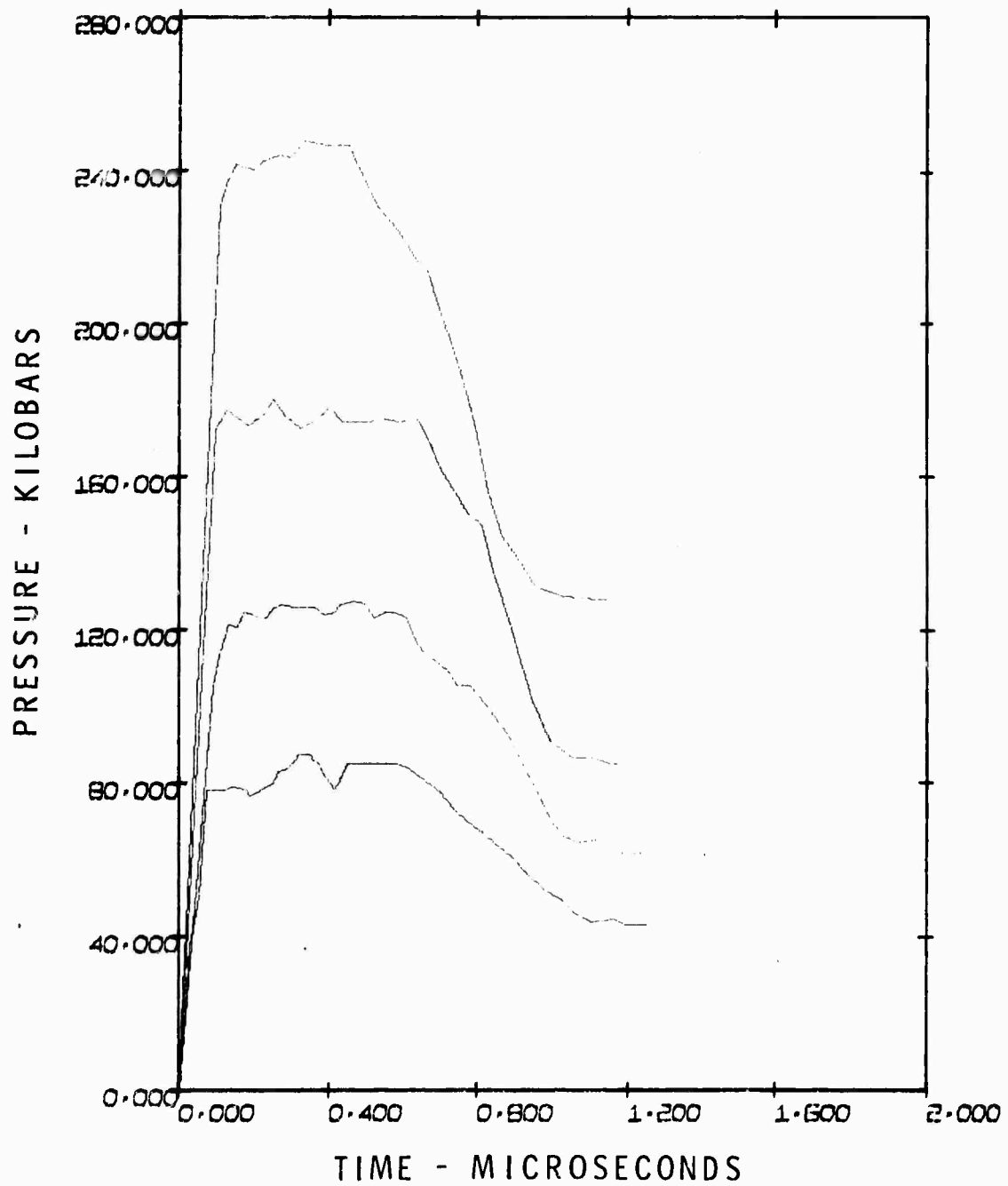


Figure 26 Aluminum Manganin Wire Records

MSL-70-01

thickness plane, the effect of increased release wave velocity with increased initial particle velocity may be seen (Figure 27). The overtaking points become progressively smaller for increasing free surface velocity, indicating higher release wave velocities. The initial rate of decrease is greater for the initially higher stress states.

Although the elastic-plastic nature of the release wave is fairly clear in the stress-time record of the manganin wire record, it is not discernable in the particle velocity or free surface velocity versus target thickness presentation. Based upon these results, it would be very difficult to detect elastic-plastic behavior from experiments measuring free surface velocity as a function of target thickness.

In Figure 28 the manganin records have been translated into stress-strain release paths. Also shown is the Hugoniot for 6061-T6 aluminum. The release paths start from points on the Hugoniot and in all cases drop below the Hugoniot. This indicates an elastic-plastic release, as a hydrodynamic release would run above the Hugoniot. Once again, because of the plastic backing plate, the paths cannot be followed to zero stress. The offset from the Hugoniot of the release path increases with increasing pressure. If the difference between the Hugoniot and the release path is taken to be $4/3Y$, then we have the following values of the yield as a function of pressure.

Peak Pressure kbar	Y kbar
0	3
76	3
111	5
163	6
237	8

MSL-70-01

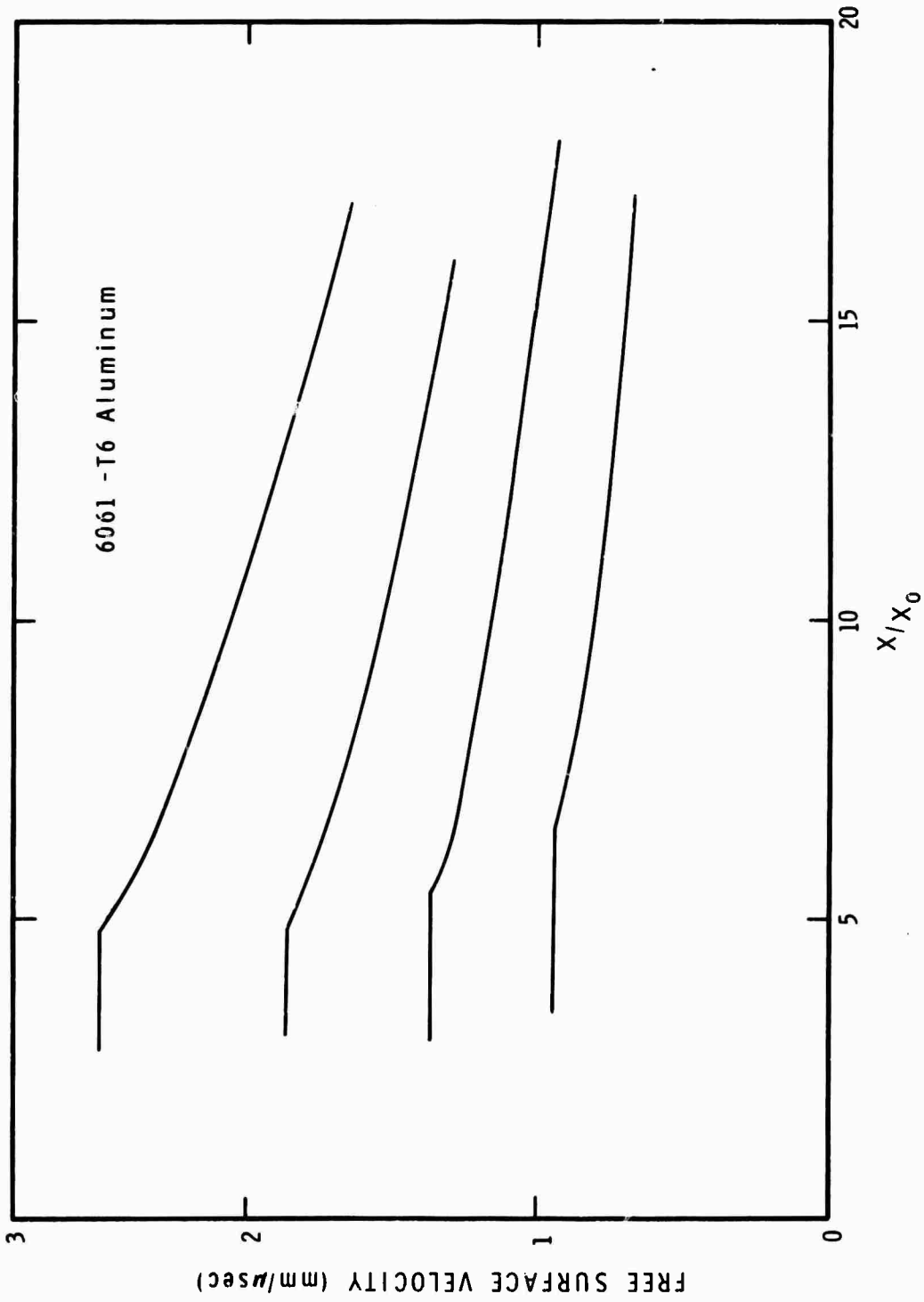


Figure 27 Free Surface Velocity vs Distance for Aluminum from Manganin Wire Gage Records

MSL-70-01

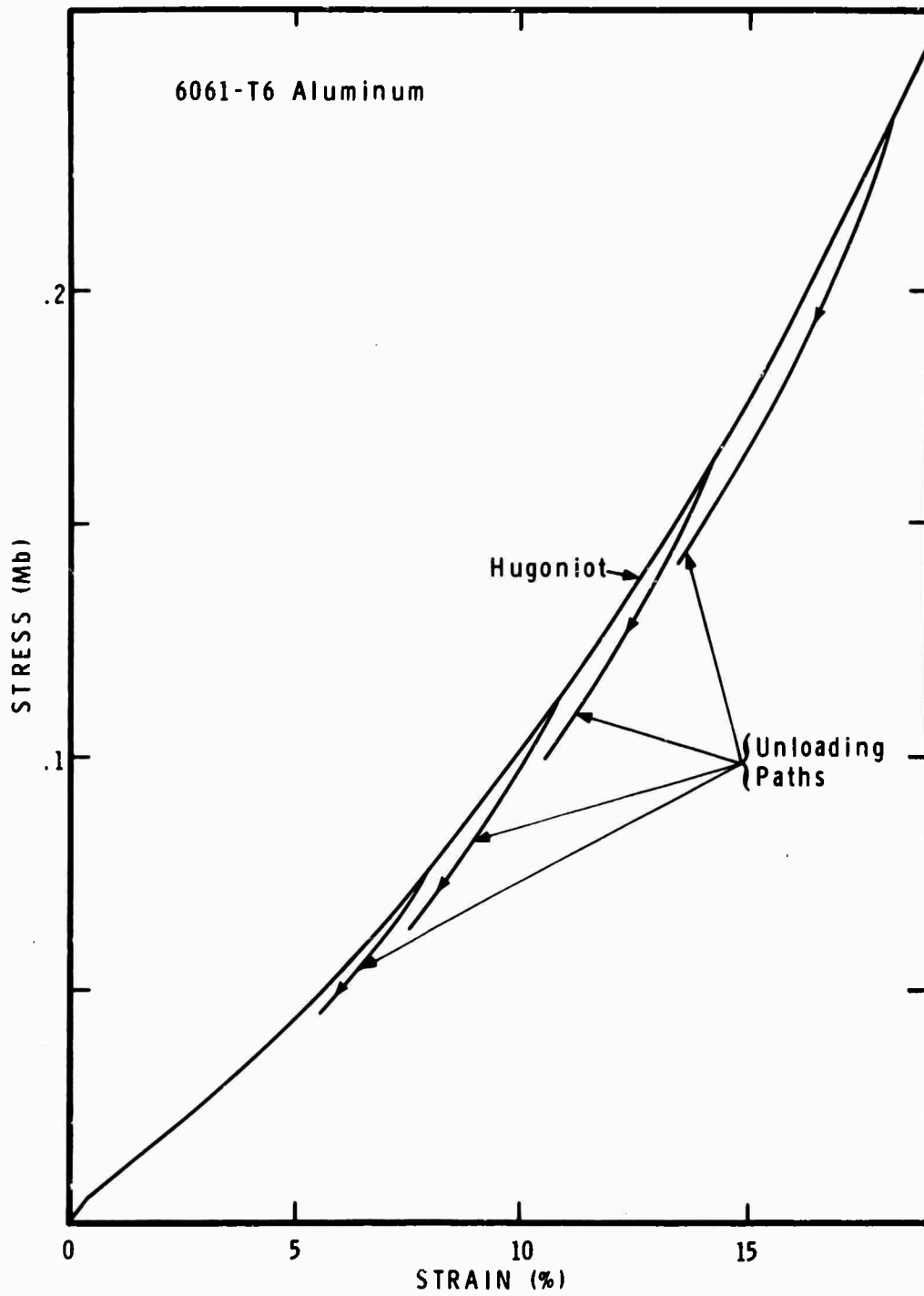


Figure 28 Aluminum Stress-Strain Release Paths from Manganin Wire Gage Records

Measurements made at higher pressures utilized the free surface method. Experiments were performed at nominal impact pressures of 8.24, 0.24, and 1.01 Mbars. Only the release wave overtaking points were measured at the higher pressures. The results of the lower pressure experiments are shown in Figure 29. Also shown in this figure is the hydrodynamic prediction of attenuation.

A comparison of the free surface velocity data and the manganin wire results are also shown in Figure 29. The manganin wire results have been projected by characteristics into the particle velocity-distance plane for this comparison. The manganin wire results agree with the free surface measurements on the location of the overtaking but not upon the rate of attenuation. The free surface velocity measurements indicate a faster rate of attenuation.

The normalized attenuation versus distance for aluminum is shown in Figure 30. Again, as with copper, the overtaking distance decreases with increasing pressure. For the range of pressures shown here, 0.076 to 0.24 Mbars, the initial rate of attenuation seems to be the same. The attenuation curves seem to be offset vertically in relative particle velocity by the same amount for the range of distances shown.

A number of high pressure experiments were performed with 6061-T6 aluminum. From these experiments only approximate values of the release wave velocity could be obtained. The values obtained indicate that the initial release from pressure levels of 0.69 and 1.01 Mbars is elastic. This may be seen in Figure 31 where the release wave velocities measured in this work and others are compared. The high pressure points fall above the release wave velocities determined by Al'tshuler et al.⁽¹⁾ indicating an initial elastic release.

MSL-70-01

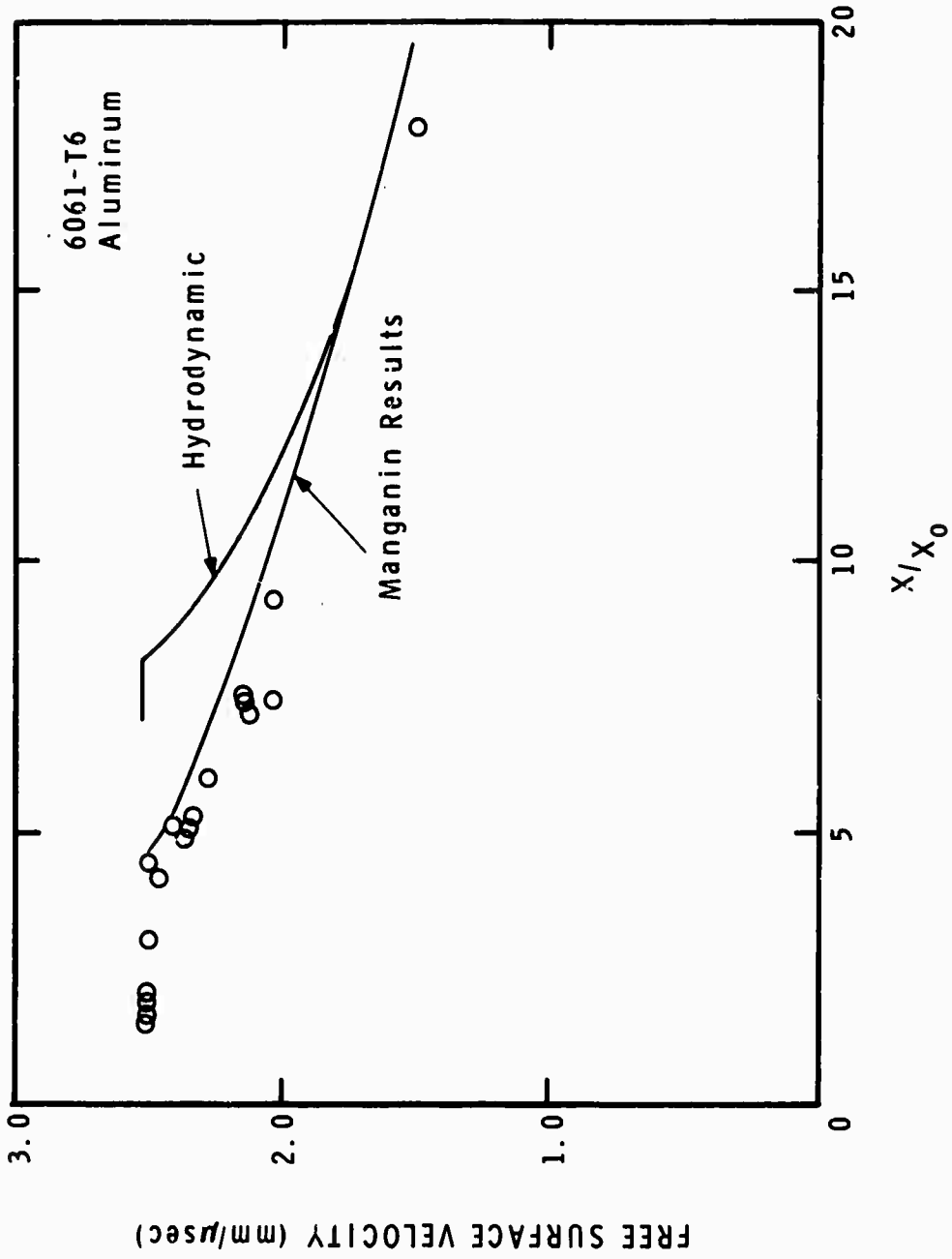


Figure 29 Free Surface Velocity vs Distance for Aluminum-2.5 mm/μsec
 Impact Velocity, Normalized to $U_{fs}=2.5$ at $X/X_0=2$, Pulse
 Length 0.14 μsec

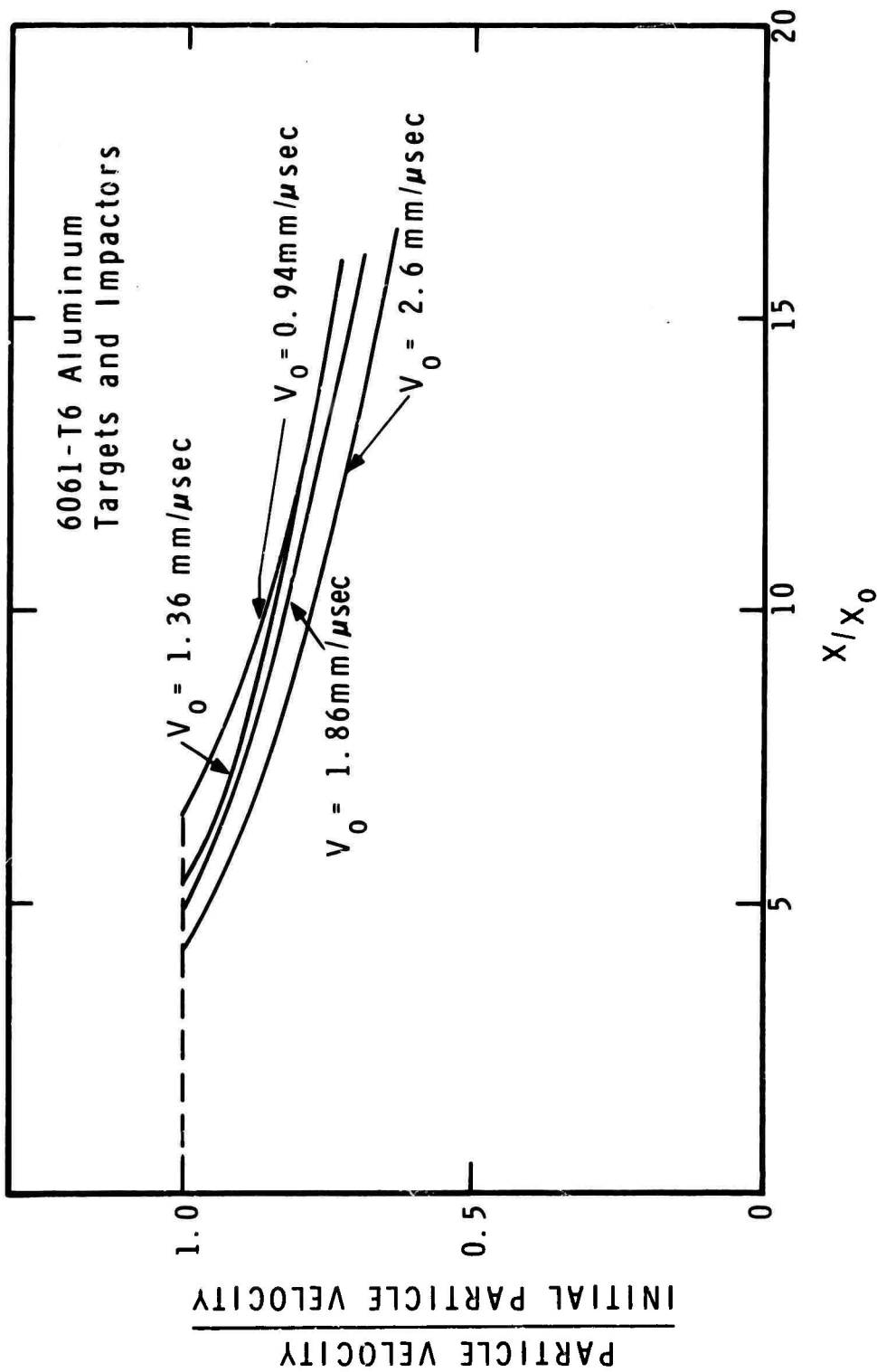


Figure 30 Normalized Attenuation for Aluminum

MSL-70-01

Two calculated plastic release wave velocity curves are shown in Figure 31. Both were calculated from the Mie-Gruneisen equation of state and the linear fit to the huginot as described by Equation 8. The upper curve was calculated using the linear fit of Al'tshuler, et al.⁽¹⁷⁾

$$D = 5.341 + 1.353 u \quad (9)$$

where D is the shock velocity

u is the particle velocity.

This is shown to demonstrate the agreement between the Russian experimental release wave points and the calculation based on their linear fit. The velocity of the first release wave observed at the highest pressure level in this work is significantly higher than the expected plastic release wave velocity. This result is taken to imply that the first release wave at this pressure level is elastic.

The evidence from the experiments with 6061-T6 aluminum at stress levels up to 0.25 Mbars show that the initial release wave is elastic and that the magnitude of the elastic wave increases with increasing pressure although the elastic release wave is not well separated from the plastic release wave. At pressures between 250 kbars and one Mbar, the initial release is believed to be elastic on the basis of the comparison with plastic release wave velocity. The elastic release wave velocity starts initially about 20% higher than the plastic release wave velocity predicted by hydrodynamics, continues to increase at that rate, and then the final two points tend back toward plastic release wave velocity.

Note that the various alloys of aluminum represented in Figure 31 cannot be distinguished (within experimental error) by their initial release wave velocities.

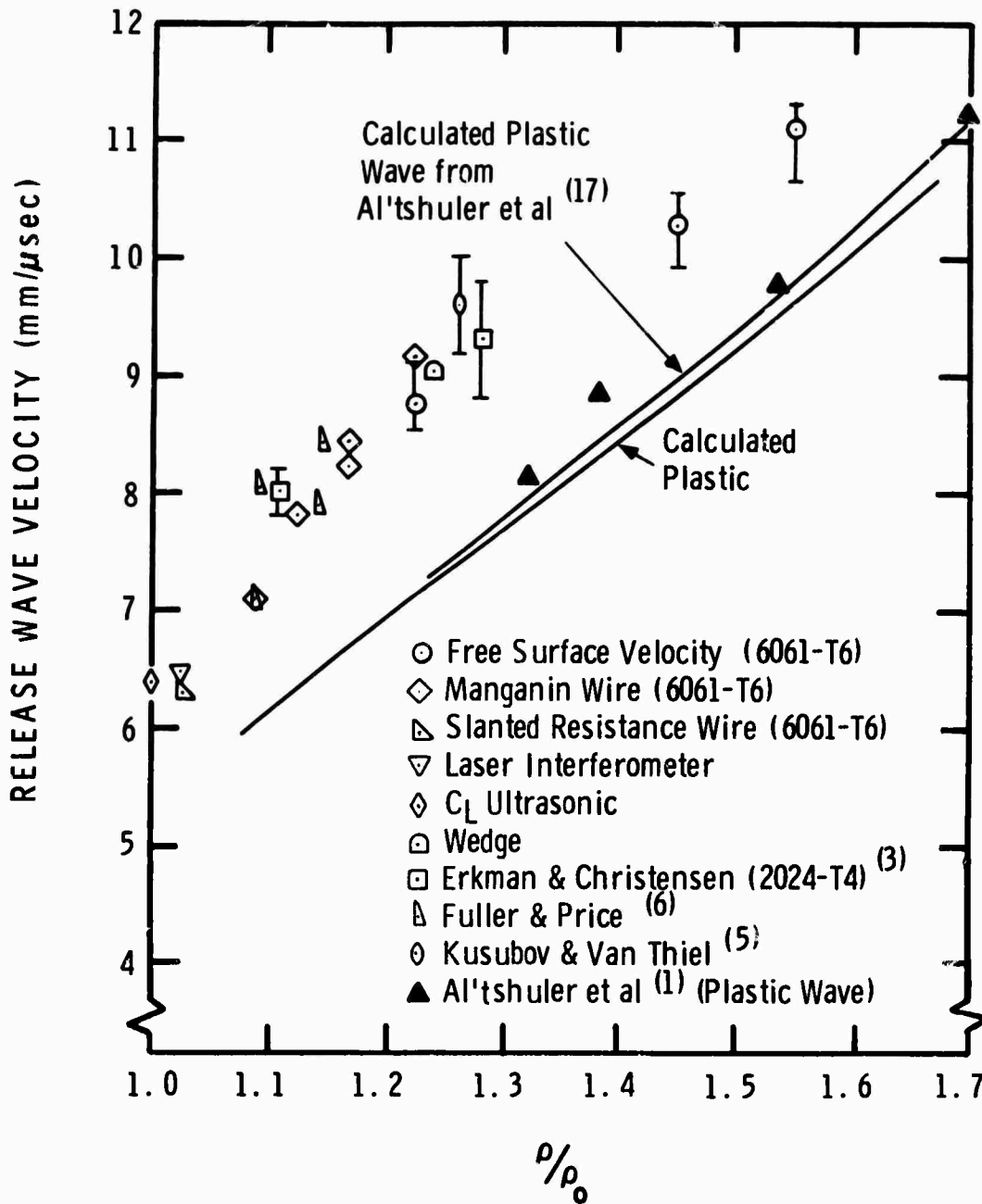


Figure 31 Release Wave Velocity vs Compression for Aluminum

MSL-70-01

TITANIUM

Two types of titanium were examined, an alloy (6Al-4V annealed) and .995 pure titanium in the α phase. Only free surface velocity and wedge experiments were performed with the 6Al-4V alloy and only manganin wire gage experiments with the α titanium.

Figure 32 presents a manganin wire record for the α titanium. Examination of the front of the wave shows a slow rise (due in part to the gage response time) and some unevenness on the top of the record due to system noise. The release wave shows a smooth transition from elastic to plastic behavior. This record was typical of the records obtained for α titanium at pressures of 80 and 134 kbar.

The manganin wire records have again been projected into the stress-strain plane (in Figure 33). Here the Hugoniot has been extrapolated downward from the high pressure Hugoniot and does not reflect a possible phase transition in this material at approximately 100 to 120 kbars. The release path shows a large offset from the Hugoniot and, if taken to be $4/3 Y$, the value of the yield is approximately 8.5 kbars. This can be compared to a quasistatic compressive yield strength of about 5 kbars. However, this material is very strain rate sensitive and shows a compressive yield of about 8 kbars when loaded at a rate of 600/sec. Stress-strain tests have also shown that the yield is significantly reduced when the temperature is increased. The manganin wire gage results probably represent a mixture of the two effects, i.e., increase of the yield point due to rate of loading and pressure and reduction of the yield point due to shock heating.

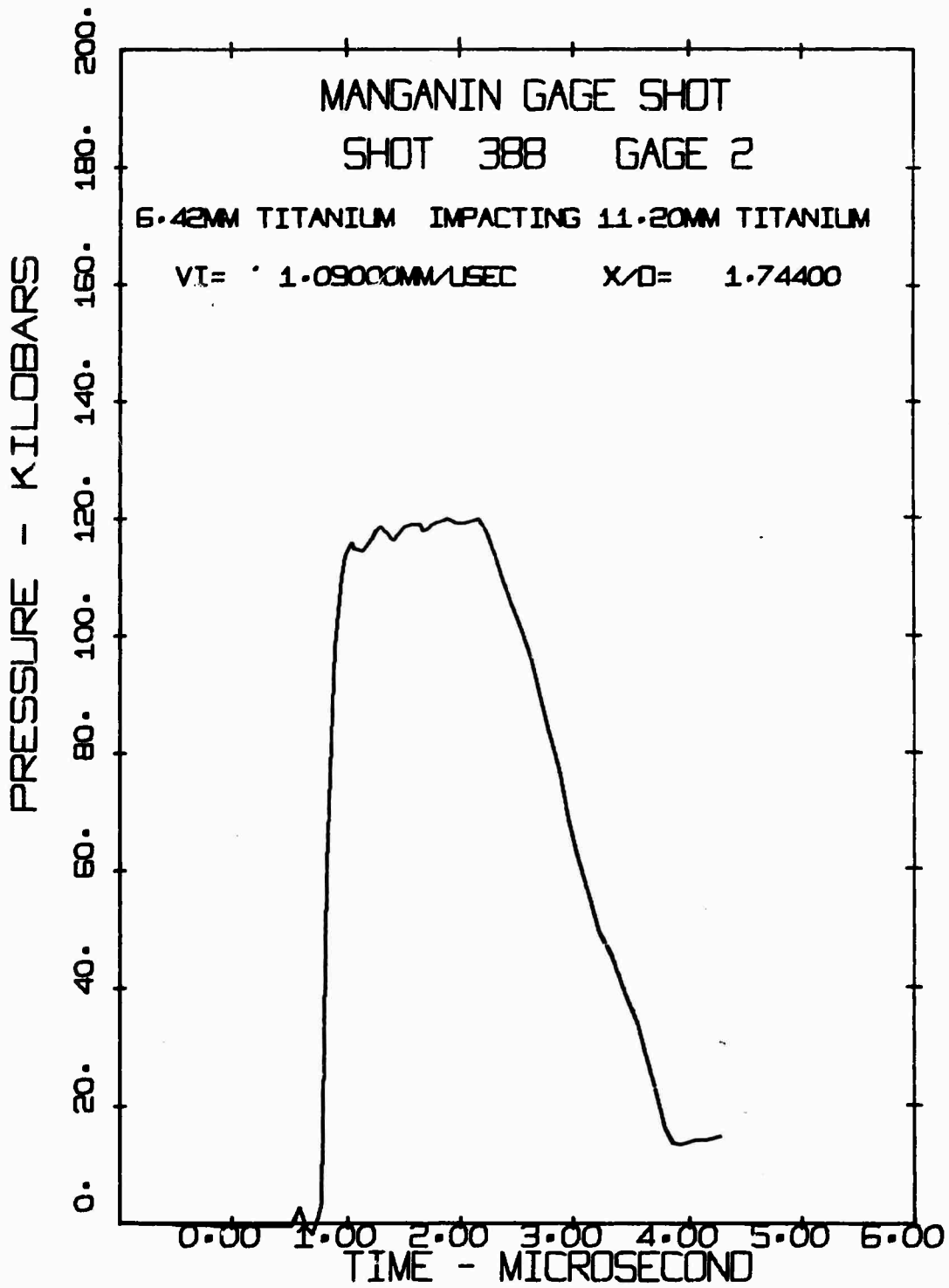


Figure 32 α Titanium Manganin Wire Record

MSL-70-01

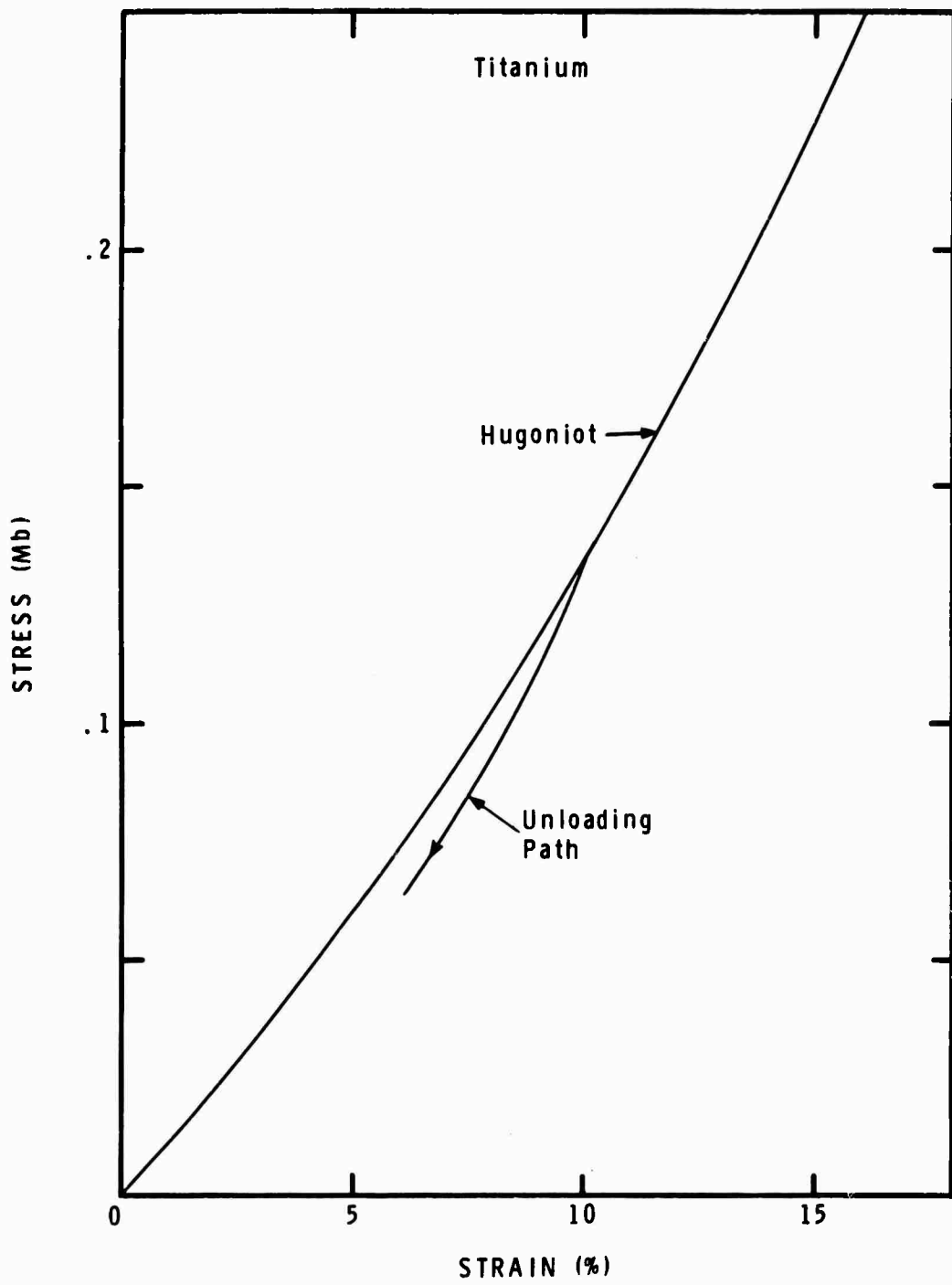


Figure 33 α Titanium Stress-Strain Release Path from Manganin Wire Gage Record

Additional data were obtained for an alloy of titanium 6Al-4V. This is a high strength material with a compressive yield strength of about 9.6 kbars, moderately ductile (13% elongation) and strain rate sensitive. Free surface velocity measurements were made at a nominal impact velocity of 2.6 mm/ μ sec. The results of these experiments are shown in Figure 34. The results suggest a gradual decrease in free surface velocity up to X/X_0 of about 7 followed by a sharp decrease. A subsequent experiment performed with a wedge gave no clear indication of this behavior. Further, since the manganin wire records gave no indication of this behavior with the pure titanium it is concluded that the gradual initial decrease in the free surface data is only an apparent effect probably caused by data scatter.

The overtaking point as determined by the wedge experiment agrees very well with the free surface velocity data.

Figure 35 presents the initial release wave velocities observed in the titanium versus relative compression. Also shown here is the calculated plastic release wave velocity. As in the case of the aluminum alloys, the data from the 6Al-4V alloy and the pure α titanium are, within experimental error, the same. The initial difference between the calculated plastic release wave velocity is quite large but appears to have decreased at a compression of 1.27.

MSL-70-01

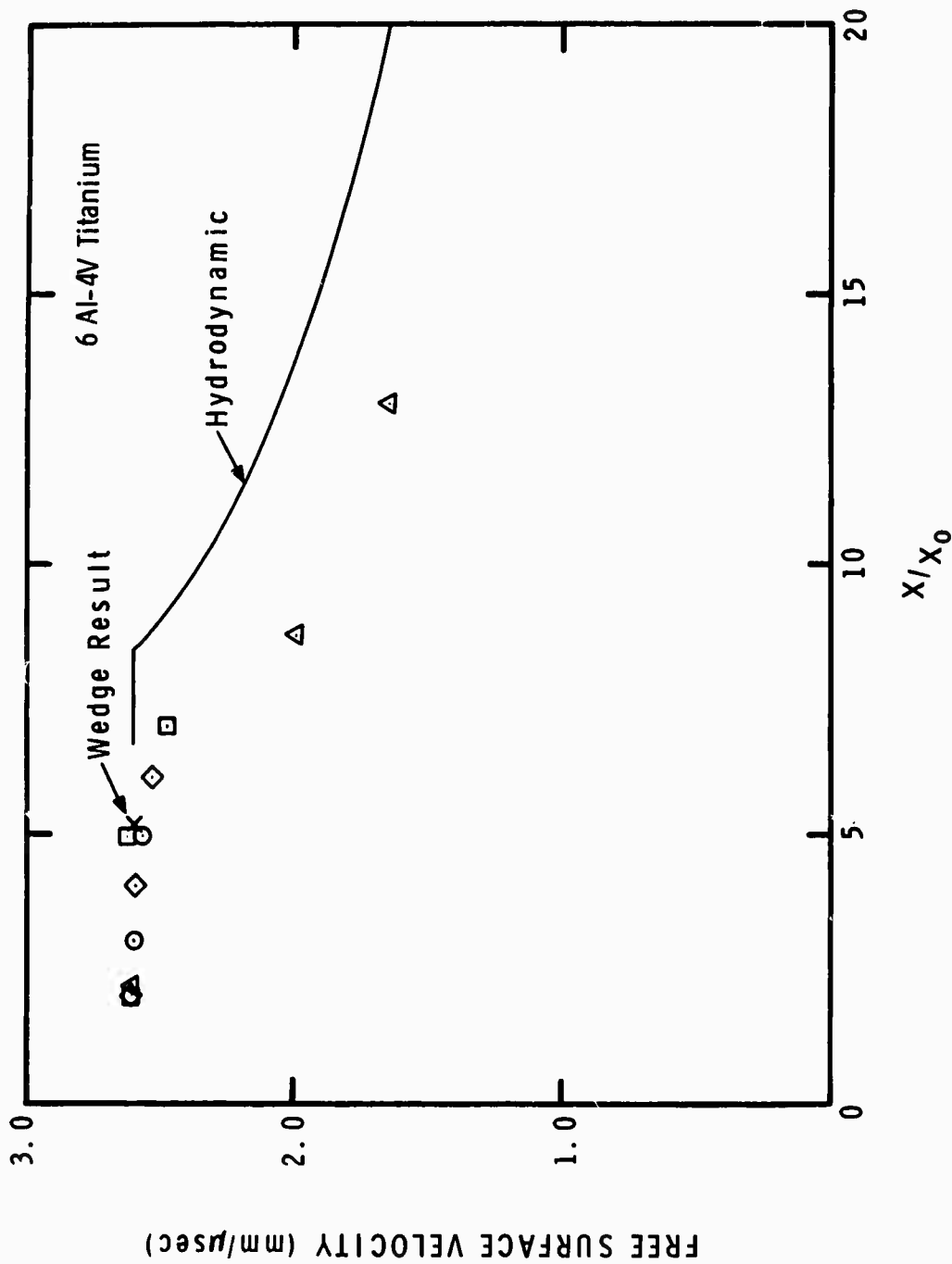


Figure 34 Free Surface Velocity vs Distance for Titanium-2.6 mm/μsec Impact Velocity, Normalized to $U_{fs}=2.6$ at $X/X_0=2$, Pulse Length 0.17 μsec

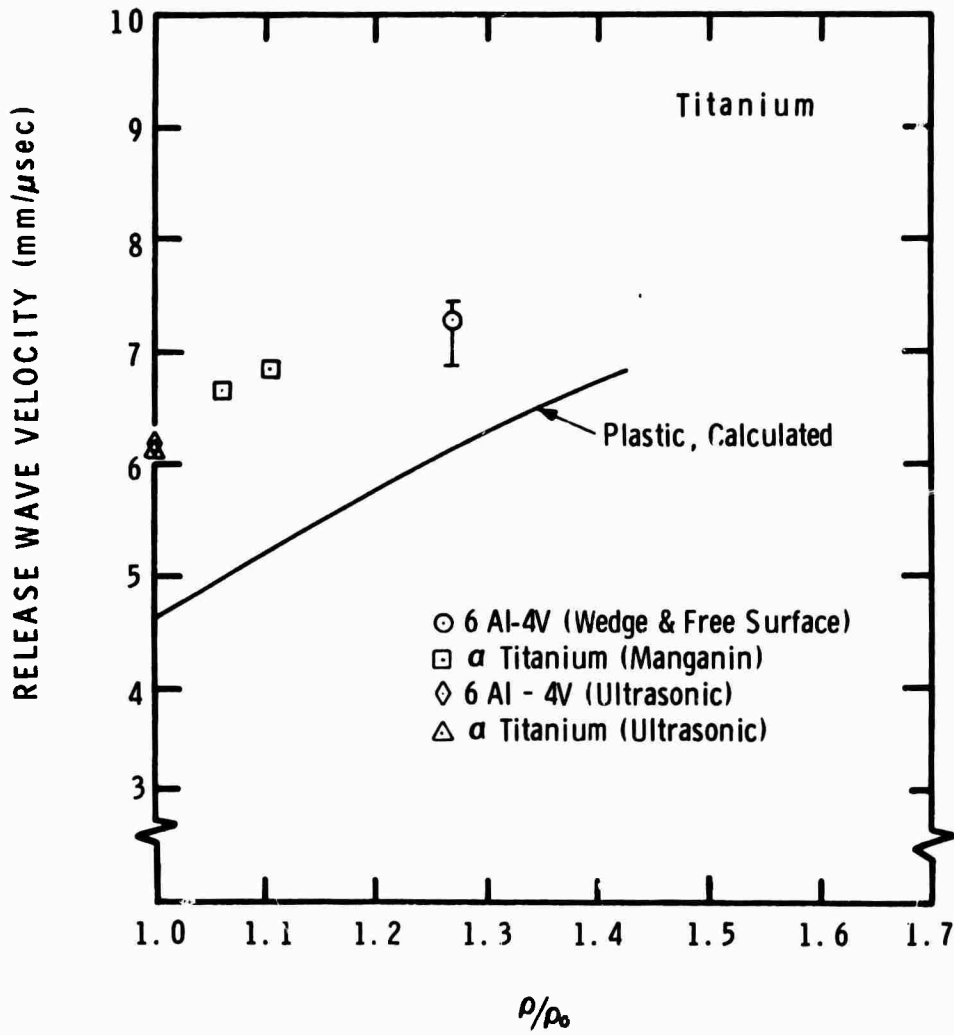


Figure 35 Release Wave Velocity vs Compression for Titanium

MSL-70-01

BERYLLIUM

Two types of beryllium were examined under the program, a wrought beryllium (similar to Brush QMV) supplied by Lawrence Radiation Laboratory and S-200 beryllium. Because of the high angle of intrusion of the lateral release waves the targets were constructed with only two steps, rather than three as employed with targets made of the other materials. The data from the experiments are presented in Figure 36 for both materials. Within experimental error there appears to be no difference in the results for the two materials. These data show a gradual decrease in free surface velocity at X/X_0 values of 1 to 3.5 then a sharp decrease at X/X_0 of about 4.5. The sharp decrease is interpreted to be the arrival of the elastic release wave from the rear surface of the impactor plate. By using an overtaking distance of X/X_0 of 4.2 with a shock velocity of 9.6 mm/ μ sec an elastic release wave velocity of 13.6 mm/ μ sec is inferred.

It is not clear why the gradual decrease in free surface velocity occurs between values of X/X_0 of 1 to 3.5. Close examination of the experiments and the results show that this decrease is a real effect since it is regular and was observed in all experiments. The accuracy of the individual experiments is $\pm 2\%$. The data show decreases outside this range. The shims used on the target surface in all experiments were of aluminum foil. These aluminum shims were observed to fly off the beryllium surface with a velocity approximately three to four percent lower than the beryllium impactor velocity. This is the expected difference due to the impedance mismatch between the beryllium and the aluminum at 225 kbars. The decrease in the free surface velocity may be due to shock dispersion, a rate effect or twinning.

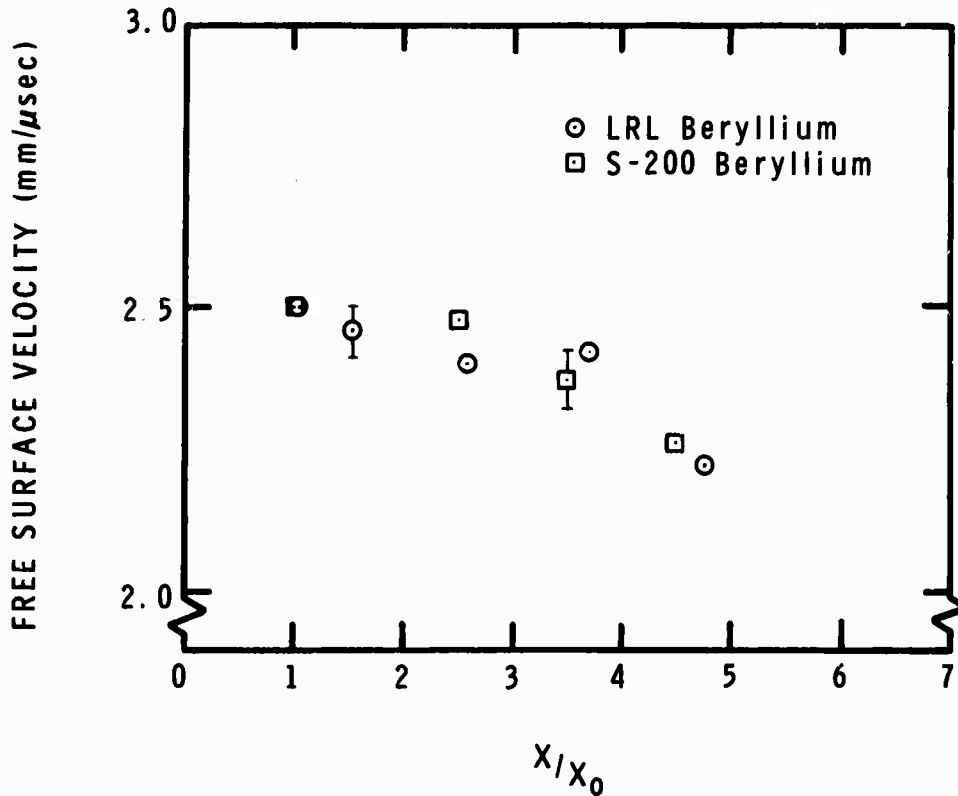


Figure 36 Free Surface Velocity vs Distance for Beryllium-2.5 mm/sec Impact Velocity, Normalized to $U_{fs}=2.5$ at $X/X_0=1$, Pulse Length 0.11 μ sec

Two sources of possible error were examined for their effect on measured velocities. The data were examined to determine if the elastic precursor was affecting the results. The free surface velocity was measured by measuring the time required for the thin surface shim to cross a small gap of known width. The initial motion of the shims was detected by their loss of reflectivity. If the elastic precursor was causing the change in reflectivity (with resulting low free surface velocities) the measured shock velocities in the specimens would be the

MSL-70-01

elastic precursor velocity. Because the shock velocity observed in all experiments corresponded to the plastic wave velocity, it was concluded that the signal of initial motion of the shim as recorded in the experiments was caused by the plastic wave. The possibility that the elastic precursor, although undetected, caused the surface to move prior to the arrival of the plastic wave was also examined. It was found that the motion due to the elastic precursor would cause a reduction of about 0.2% in the gap width for the experiments performed and an increase in the free surface velocity of the same amount. Therefore, the observed effect is associated with the plastic portion of the compressive wave.

URANIUM ALLOY

A limited group of experiments were performed using impactor plates and targets of a uranium alloy supplied by Lawrence Radiation Laboratory. The density of this alloy was 16.41 grams/cm³.⁽¹⁶⁾ Cooper shims were used in these experiments. The results of the experiments are shown in Figure 37. These data indicate an overtaking distance of X/X_0 of about 4.8. This taken with a particle velocity of 1.26 mm/μsec and a shock velocity of 4.46 mm/μsec gives a release wave velocity of 4.88 mm/μsec.

The data is somewhat suspect because it is felt that the impactor plates were broken prior to impact. Examination of the streak camera records of the experiments showed unexplained discontinuities in the traces. An experiment was performed in which a plate of the uranium alloy was impacted directly upon the reflecting surface of a mirror, and the mirror observed with the streak camera. The record from this experiment

showed that the impactor plate was not flat upon impact and indicated that it was broken in the center. Subsequent experiments of the same type were attempted using stronger backing plates behind the uranium plate and lower launch velocities without success.

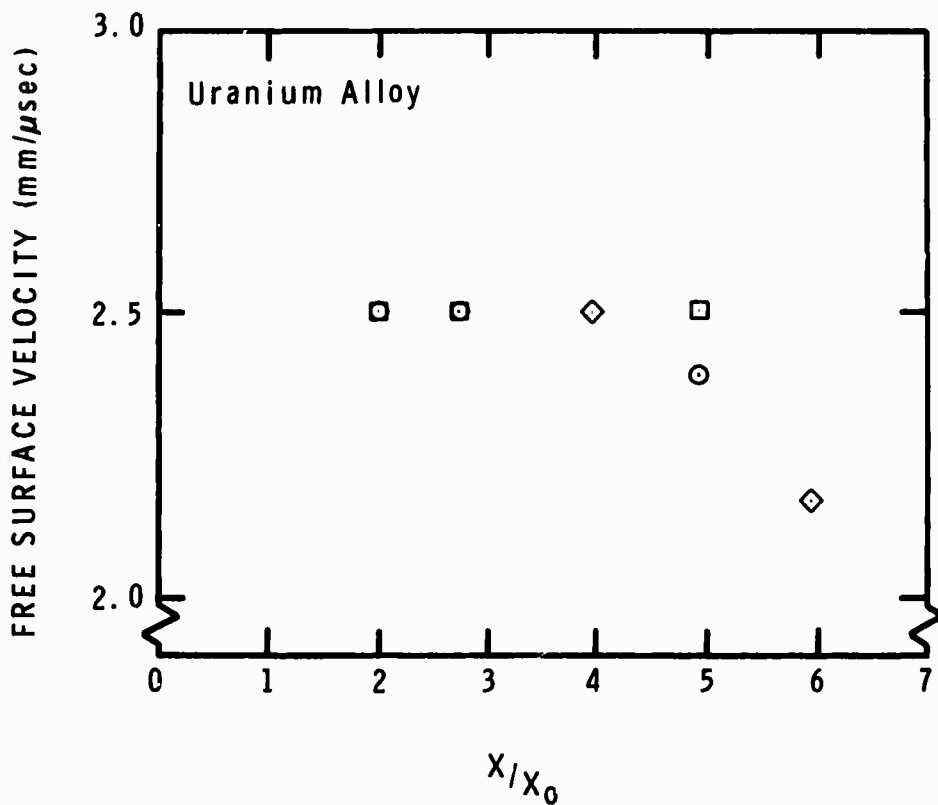


Figure 37 Free Surface Velocity vs Distance for Uranium Alloy-2.5 mm/ μ sec Impact Velocity, Normalized to $U_{fs}=2.5$ at $X/X_0=2$, Pulse Length 0.23 μ sec

MSL-70-01

SECTION IV

CONCLUSIONS

From the preceding experimental results several conclusions may be drawn:

1. For all materials examined elastic release wave behavior observed. For those materials for which pressure-time profiles were recorded, increases in strength were observed with increases in pressure. The presence of significant shear strengths was observed through comparison of observed sound velocities with the observed or calculated plastic release wave velocities as in Figure 38. The velocity of the first observed disturbance is compared to plastic release wave velocity. Most of the data cluster about a line of slope 1.2. Data significantly below the 1.2 slope line are expected when the temperature behind the shock front becomes sufficient to melt the material in the compressed state and the shear strength becomes zero. Elastic waves will then no longer be observed. McQueen, et al.⁽¹⁸⁾ calculate the onset of melting for copper to be at a pressure of 1.33 Mbars. The upper two copper points shown in Figure 38 above this pressure and fall about a line of slope equal to one. Since this represents plastic release wave velocity we take this to indicate melting behind the shock front. The highest pressure point for aluminum (1.01 Mbar) indicates elastic release. Urlin⁽¹⁹⁾ has predicted melting to occur in aluminum at approximately 1 Mbar. These experimental results indicate that melting has not yet

MSL-70-01

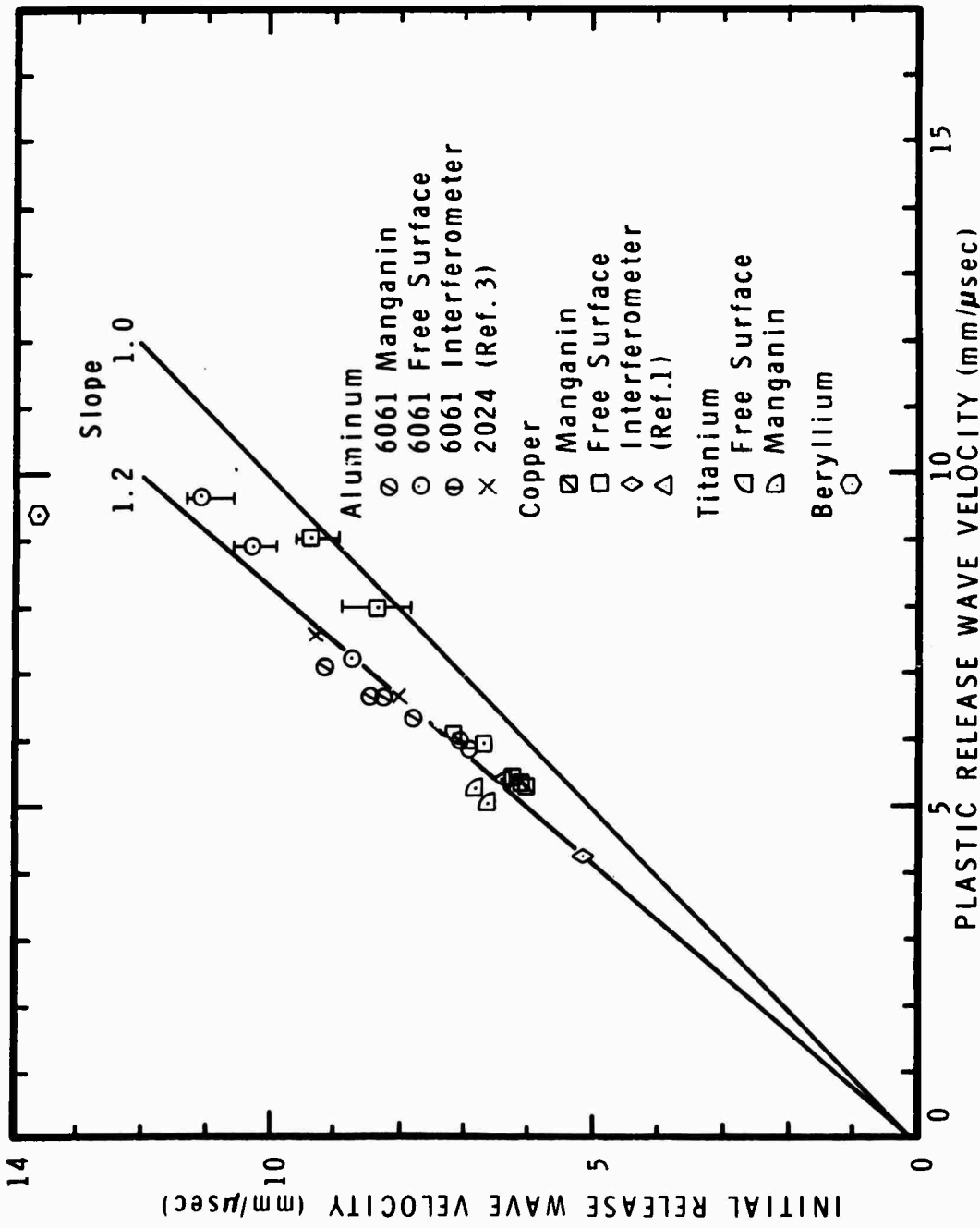


Figure 38 Initial Release Wave Velocity vs Plastic Release Wave Velocity

MSL-70-01

occured at this pressure. The difference in melting characteristics of the alloys of aluminum may account for this behavior, however.

With the exception of beryllium (see below) and the two copper points, all the points fall about the 1.2 slope line indicating no melting behind the shock front.

Because shock wave velocity is approximately equal to plastic release wave velocity, the fact that data cluster about a line of slope 1.2 provides the basis of approximating elastic release wave velocities for materials whose release wave properties are not known.

The observed increase of strength followed by an eventual loss of strength when melting is approached suggests that the two effects, heating and increasing strength, are in competition. For pressures where there is little shock heating the material strength increases. As the pressure is increased, heating produces a slower rate of increase in elastic strength and finally a decrease to essentially no strength when melting occurs. For this behavior there would be a pressure at which the material would show a maximum strength.

2. In none of the materials examined was elastic-perfectly plastic behavior clearly observed. From the stress-strain release paths it is concluded that the Bauschinger effect was observed for copper, α titanium and 6061-T6 aluminum. From the free surface velocity experiments with other materials it was not possible to separate elastic and plastic release waves.

3. Examination of the results shown in Figure 38 leads to the conclusion that, Poisson's ratio (ν) is not a strong function of pressure and temperature up to the onset of melting. Further the elastic release wave velocity is related to plastic release wave velocity by

$$\frac{C_e}{C_p} = \left(\frac{3(1-\nu)}{1+\nu} \right)^{1/2} \quad (10)$$

For the materials shown in Figure 35, ν is approximately .3 which leads to a ratio or slope of about 1.24. Beryllium is a significant departure from this with $\nu = .055$.

The beryllium ratio of elastic to plastic wave speeds is predicted to be 1.64 and 1.41 is observed indicating a decrease in Poisson's ratio.

4. From the results of the experiments and other data such as shown in Figure 35, alloys of metals show little difference in their elastic release wave velocities, at the high pressures tested. This does not imply that the details of the release waves are the same.
5. Through the course of the experimental program it became clear that without pressure-time or particle velocity-time measurements it is very difficult, if not impossible, to identify elastic-plastic behavior. Examination of the pressure-time plots and the resulting projections into free surface velocity-distance plots demonstrates that the elastic-plastic release waves observed in the pressure-time plots are not clearly shown in the free surface velocity-distance plane.

MSL-70-01

Experiments with wedges were useful only to identify the overtaking of the shock front by the first release wave. Extraction of attenuation data from wedge results requires differentiation of the data, which results in errors that can obscure the rate of attenuation. Examination of this problem revealed also that wedge experiments can be an extremely delicate measure of wave curvature or impactor curvature. Extremely small curvature of the impactor plate can obscure the rate of attenuation.

This work has shown that elastic release waves persist to very high pressures. The significance of these high pressure elastic release waves in attenuation should be further evaluated.

REFERENCES

1. Al'tshuler, L. V., Kormer, S. B., Brazhnik, M. I., Vladimirov, L. A., Speranskaya, M. P. and Funtikov, A. I., Soviet Physics, JETP, Vol. 11, No. 4, p. 766-775, October, 1960.
2. Curran, D. R., J. Appl. Phys., Vol. 34, No. 9, p. 2677-2685, September, 1963.
3. Erkman, J. O. and Christensen, A. B., J. Appl. Phys., Vol. 38, No. 13, p. 5395-5403, December, 1967.
4. Barker, L. M., "Fine Structure of Compressive and Release Wave Shapes in Aluminum Measured by the Velocity Interferometer Technique", Behavior of Dense Media Under High Dynamic Pressures, Gordon and Breach, New York 1968, p. 483-505.
5. Kusubov, A. S. and VanTheil, M., J. Appl. Phys., Vol. 40, No. 9, p. 3776-3780, August, 1969.
6. Fuller, P. J. A. and Price, J. H., Brit., J. Appl. Phys., Series 2, Vol. 2, p. 275-286, 1969.
7. Lingle, R. and Jones, A. H., TR65-65, GM Defense Research Laboratories, Santa Barbara, California, September, 1965.
8. Lyle, J. W., Schriever, R. L. and McMillan, A. R., J. Appl. Phys., Vol. 40, No. 10, p. 4663-4664, 1969.
9. Fowles, G. R. and Isbell, W. M., J. Appl. Phys., Vol. 36, No. 4, p. 1377-1379, 1965.
10. Isbell, W. M. and Christman, D. R., "Shock Propagation and Fracture in 6061-T6 Aluminum from Wave Profile Measurements", Materials and Structures Laboratory, Manufacturing Development, General Motors Corporation, Warren, Michigan, MSL-69-70, 1970.
11. Isbell, W. M., Christman, D. R., Babcock, S. G., Michaels, T. E. and Green, S. J., "Measurements of Dynamic Properties of Materials-Vol. I-Summary of Results", Materials and Structures Laboratory, Manufacturing Development, General Motors Corporation, Warren, Michigan, MSL-70-23, Vol. I, 1970.

MSL-70-01

12. Green, S. J. and Schierloh, F. L., "Uniaxial Stress Behavior of S-200 Beryllium, Isotropic Pyrolytic Boron Nitride and ATJ-S Graphite at Strain Rates to 10^3 /Second and 700°F", Materials and Structures Laboratory, Manufacturing Development, General Motors Corporation, Warren, Michigan, MSL-68-11, 1968.
13. Munson, D. E., "Dynamic Behavior of Beryllium", Sandia Laboratories, Albuquerque, New Mexico, SC-RR-67-368, 1967.
14. McQueen, R. G., Marsh, S. P., Taylor, J. W., Fritz, J. N. and Cuter, W. J., "The Equation of State of Solids from Shock Wave Studies", High-Velocity Impact Phenomena, Ed. by R. Kinslow, Academic Press, New York, 1970.
15. Isbell, W. M., Shipman, F. H. and Jones, A. H., "Hugoniot Equation of State Measurements for Eleven Materials to Five Megabars", Materials and Structures Laboratory, Manufacturing Development, General Motors Corporation, Warren, Michigan, MSL-68-13, 1968.
16. Royce, E. B. and Gust, W. H., "Shock Compression of the Stainless Uranium Alloy Mulberry", Lawrence Radiation Laboratory, University of California, Livermore, California, UCRL 50888, 1970.
17. Al'tshuler, L. V., Kormer, S. B., Bakanova, A. A. and Trunin, R. F., Soviet Physics, JETP, Vol. 11, No. 4, p. 573, 1966.
18. McQueen, R. G., Carter, W. J., Fritz, J. N. and Marsh, S. P., "The Solid-Liquid Phase Line In Cu", presented at the Symposium on the Accurate Characterization of High Pressure Environment, U.S. Dept. of Commerce, National Bureau of Standards, Gaithersburg, Maryland, October 14-18, 1968.
19. Urlin, V. D., Soviet Physics, JETP, Vol. 22, No. 2, p. 341-346, 1966.